High-Performance Concrete Comprising Silica Fume: Evaluation of the Decommissioned Salt Lake City Airport Parking Structure

Trevor William Pratt

A thesis submitted to the faculty of
Brigham Young University
in partial fulfillment of the requirements for the degree of

Master of Science

W. Spencer Guthrie, Chair
Johnn Judd
Amanda Bordelon

Department of Civil and Construction Engineering

Brigham Young University

ABSTRACT

The objective of this research was to quantify the benefits of silica fume through a detailed investigation of the concrete decks within the now-demolished Salt Lake City International Airport parking structure, which was constructed in 1991, after it had been in service for almost 30 years. Several tests were performed to evaluate each of five areas within the parking structure. The results of field testing included data obtained from visual inspection, chain dragging, Schmidt hammer testing, and cover meter readings, while the results of laboratory testing included data obtained from chloride concentration, modulus of elasticity, electrical impedance, rapid chloride permeability, splitting tensile strength, compressive strength, and carbonation depth testing.

The concrete comprising silica fume exhibited higher average values than concrete without silica fume in Schmidt hammer, electrical impedance, and compressive strength testing and lower average values than concrete without silica fume in chloride concentration, RCPT, and carbonation depth testing; these results suggest that concrete comprising silica fume would provide greater strength and durability than concrete without silica fume. As exceptions, concrete without silica fume exhibited marginally higher values than concrete comprising silica fume in modulus of elasticity and splitting tensile strength testing.

The results of this research suggest that concrete comprising silica fume should be expected to provide greater strength and durability than concrete without silica fume, assuming that the concrete mixture is designed, produced, placed, and cured properly. Where budgets permit, silica fume is therefore recommended for concrete projects for which high strength and durability are needed. Further research would be beneficial in comparing the performance of concrete comprising silica fume and concrete without silica fume in other applications, as well.

Keywords: chloride, concrete, durability, parking structure, silica fume, strength

ACKNOWLEDGEMENTS

The author acknowledges the extraordinary amount of help from Dr. Spencer Guthrie in completing this project. Dr. Amanda Bordelon of Utah Valley University also helped immensely. Research assistants Natalie Sumsion, Ammon Hymas, and Brindalynn Darby, of the Brigham Young University (BYU) Department of Civil and Construction Engineering, assisted in collecting samples from the parking structure. Dr. Brian Mazzeo and research assistant Enoch Boekweg, of the BYU Department of Electrical and Computer Engineering, were instrumental in gathering data regarding electrical impedance of the concrete. Dr. Tenli Waters Emery assisted in collecting samples and training the author how to analyze such samples. The American Concrete Institute (ACI) Foundation and Utah Department of Transportation are recognized as the primary financial sponsors for this project. Finally, the author expresses extreme thanks to his family and all those who have been supportive in accomplishing this goal.

TABLE OF CONTENTS

LIST OF TABLES ..... *vi*
LIST OF FIGURES ..... *vii*
1 INTRODUCTION 1
1.1 Problem Statement 1
1.2 Research Objective and Scope of Work 1
1.3 Outline of Report 2
2 BACKGROUND 3
2.1 Overview 3
2.2 Origin of Silica Fume 3
2.3 Use of Silica Fume in Concrete 3
2.4 Concrete Deterioration Mechanisms 5
2.5 Summary 6
3 PROCEDURES 7
3.1 Overview 7
3.2 Testing Plan 7
3.3 Field Testing 8
3.3.1 Visual Inspection 8
3.3.2 Chain Dragging 8
3.3.3 Schmidt Hammer Testing 8
3.3.4 Cover Depth Measurements 21
3.3.5 Chloride Concentration Sampling 22
3.3.6 Coring 24
3.4 Laboratory Testing 24
3.4.1 Chloride Concentration Testing 24
3.4.2 Modulus of Elasticity Testing 24
3.4.3 Electrical Impedance Testing 28
3.4.4 Rapid Chloride Permeability Testing 28
3.4.5 Splitting Tensile Strength Testing 28
3.4.6 Compressive Strength Testing 31
3.4.7 Carbonation Depth Measurements 31
3.5 Summary 35
4 TEST RESULTS 36
4.1 Overview 36
4.2 Field Testing Results 36
4.2.1 Visual Inspection 36
4.2.2 Chain Dragging 36
4.2.3 Schmidt Hammer Testing 36
4.2.4 Cover Depth Measurements 36
4.3 Laboratory Testing Results 42
4.3.1 Chloride Concentration Testing 42
4.3.2 Modulus of Elasticity Testing 49
4.3.3 Electrical Impedance Testing 49
4.3.4 Rapid Chloride Permeability Testing 49
4.3.5 Splitting Tensile Strength Testing 49
4.3.6 Compressive Strength Testing 54

4.3.7 Carbonation Depth Measurements 54
4.4 Summary 54
5 CONCLUSION 58
5.1 Summary 58
5.2 Findings 58
5.3 Recommendations 59
REFERENCES 60
APPENDIX ORIGINAL CORES 63

LIST OF TABLES

Table 3-1: Chloride Sampling Lift and Drill Bit Diameter 23
Table 3-2: Core Designation, Location, and Tests 25
Table 4-1: Schmidt Rebound Numbers for Ground Level 37
Table 4-2: Schmidt Rebound Numbers for Entrance Ramp 37
Table 4-3: Schmidt Rebound Numbers for Second Level 38
Table 4-4: Schmidt Rebound Numbers for Third Level 39
Table 4-5 Schmidt Rebound Numbers for Helix 39
Table 4-6: Average Schmidt Rebound Numbers 39
Table 4-7: Cover Depth Measurements for Entrance Ramp 40
Table 4-8: Cover Depth Measurements for Second Level 41
Table 4-9: Cover Depth Measurements for Third Level 42
Table 4-10: Cover Depth Measurements for Helix 42
Table 4-11: Chloride Concentration Data for Ground Level 43
Table 4-12: Chloride Concentration Data for Entrance Ramp 44
Table 4-13: Chloride Concentration Data for Second Level 45
Table 4-14: Chloride Concentration Data for Third Level 46
Table 4-15: Chloride Concentration Data for Helix 47
Table 4-16: Comparison of Average Chloride Concentrations for Uncracked and Cracked Concrete 48
Table 4-17: Modulus of Elasticity Data 50
Table 4-18: Electrical Impedance Data 51
Table 4-19: Rapid Chloride Permeability Data 52
Table 4-20: Ratings of Chloride Permeability 52
Table 4-21: Splitting Tensile Strength Data 52
Table 4-22: Compressive Strength Data 55
Table 4-23: Carbonation Depth Measurements 55

LIST OF FIGURES

Figure 2-1: Silica fume powder. 4
Figure 3-1: Aerial view of parking structure. 9
Figure 3-2: Aerial view of ground-level area. 10
Figure 3-3: Schematic of ground-level area. 11
Figure 3-4: Aerial view of entrance-ramp area. 12
Figure 3-5: Schematic of entrance-ramp area. 13
Figure 3-6: Aerial view of second-level area. 14
Figure 3-7: Schematic of second-level area. 15
Figure 3-8: Aerial view of third-level area. 16
Figure 3-9: Schematic of third-level area. 17
Figure 3-10: Schematic of helix area. 18
Figure 3-11: Chain dragging 19
Figure 3-12: Schmidt hammer testing. 20
Figure 3-13: Cover depth testing. 21
Figure 3-14: Chloride concentration sampling 22
Figure 3-15: Hole dimensions for chloride concentration sampling. 23
Figure 3-16: Concrete samples. 26
Figure 3-17: Impact resonance testing. 27
Figure 3-18: Electrical impedance testing 29
Figure 3-19: Rapid chloride permeability testing. 30
Figure 3-20: Splitting tensile strength testing. 32
Figure 3-21: Compressive strength testing. 33
Figure 3-22: Carbonation depth testing. 34
Figure 4-1: Typical core after splitting tensile strength testing. 53
Figure 4-2: Typical core after compressive strength testing. 56

1 INTRODUCTION

1.1 Problem Statement

Corrosion of reinforcing steel remains a prevalent cause of failure in reinforced concrete structures (Guthrie and Yaede 2013) and can be caused by many factors, including chloride ion exposure and carbonation, for example. The permeability of concrete to chloride ions, in particular, has therefore become a useful predictor of the potential for corrosion of reinforcing steel. When concrete is more permeable, chloride ions can more easily penetrate the concrete matrix and reach the rebar (Guthrie and Yaede 2013).

Numerous studies have already demonstrated that silica fume significantly decreases the permeability of concrete (Chia and Zhang 2002, Galishnikova et al. 2020, Murthi and Sivakumar 2008, Wolsiefer 1991, Yusuf 2019). The studies explain that reductions in concrete permeability are achieved as silica fume fills microstructural voids within the concrete matrix. Nearly all of these studies, however, were experiments that were performed within a controlled laboratory environment where the test specimens were not subjected to extended environmental or loading conditions. Indeed, only two studies involved collection of field data, which was limited to rapid chloride permeability testing (RCPT) of cores removed from a parking structure (Wolsiefer 1991) and compressive strength testing, splitting tensile strength testing, and hydration analyses over a 7-year period on cylinders cast within a laboratory setting (Persson 1998). More comprehensive data on the effects of silica fume over an extended period of time, such as 30 years, were not available prior to the start of this research.

The American Concrete Institute (ACI) is interested in understanding the long-term quantitative and qualitative properties of concrete comprising silica fume. Decreases in concrete permeability resulting from the addition of silica fume can enhance concrete durability, especially in cold regions where concrete may be exposed to chloride-based deicing salts that are applied to roads and bridges as part of winter maintenance; specifically, chloride ions from deicing salts would be less able to penetrate the concrete or cause corrosion of the reinforcing steel. Reducing chloride ion ingress would therefore greatly increase the service life of the structure in these conditions (Guthrie and Yaede 2013, Hebdon 2020).

1.2 Research Objective and Scope of Work

The objective of this research was to quantify the benefits of silica fume through a detailed investigation of the concrete decks within the now-demolished Salt Lake City International Airport parking structure, which was constructed in 1991, after it had been in service for almost 30 years. Areas on the ground level, the entrance ramp to the first level, the second level, the third level, and the east helix were selected for testing. Properties of the concrete decks were analyzed through visual inspection, chain dragging, Schmidt hammer testing, cover depth measurements, chloride concentration testing, impact resonance tests, electrical impedance measurements, RCPT, splitting tensile strength testing, compressive strength testing, and carbonation depth testing.

1.3 Outline of Report

This report contains five chapters. This chapter presents the objective, scope of work, and outline of the report. Chapters 2, 3, and 4 present background information on concrete comprising silica fume, methods of experimentation, and test results, respectively. In Chapter 5, the test results are summarized, and general recommendations based on the findings are presented.

2 BACKGROUND

2.1 Overview

The following sections provide information obtained from a review of the literature about concrete comprising silica fume, including the origin of silica fume, the application of silica fume in concrete, and concrete deterioration mechanisms.

2.2 Origin of Silica Fume

Silica fume is a co-product of silicon and ferrosilicon metals (Fidjestøl and Dåstøl 2008). As gaseous silicon oxide (SiO) is exiting the smelting furnace, it reacts with oxygen in the air to form solid silicon dioxide (SiO_2). The SiO_2 particles, which are more commonly referred to as silica fume, are less than 0.00004 in. in diameter, making it an extremely fine powder; the particles are approximately one hundredth of the size of an average cement particle (Silica Fume Association 2005). The significant size difference allows the silica fume to fill microstructural voids within the concrete matrix, which in turn reduces the permeability of the concrete. The small particle size of silica fume, however, also increases the likelihood of accidental inhalation because the particulate will linger in the air longer than larger particles, such as cement (Klemetti 2012). Silica fume powder is shown in Figure 2-1.

Experiments with silica fume in concrete began in the 1940s, and the first known technical paper on concrete comprising silica fume was published in 1952 by C. J. Bernhard (Fidjestøl and Dåstøl 2008). The first recorded use of silica fume in structural concrete was in Norway in 1971, and continued applications of silica fume in concrete have motivated studies on the effects of silica fume on strength, particle packing, mitigation of the alkali-silica reaction, and carbonation depth, for example (Fidjestøl and Dåstøl 2008, Galishnikova et al. 2020, Kulakowski et al. 2009, Yusuf 2019).

2.3 Use of Silica Fume in Concrete

Similar to other supplementary cementitious materials such as fly ash, silica fume is a pozzolan that is often added to concrete as a partial replacement of portland cement. Typical replacement percentages range from 5% to 25% (Galishnikova et al. 2020). Although silica fume can be added as a powder, it can also be added as a slurry when mixed with water, which minimizes the likelihood of accidental inhalation.

As a partial replacement of portland cement, pozzolans such as silica fume facilitate the formation of additional calcium silicate hydrate (C-S-H), which is the primary binder in concrete. C-S-H is initially formed as a primary product of the portland cement hydration reaction, and additional C-S-H is formed through a pozzolanic reaction between silica fume and calcium hydroxide (CH), which is a secondary product of the cement hydration reaction. The formation of C-S-H densifies and strengthens the concrete matrix (Silica Fume Association 2005, Yusuf 2019).

Figure 2-1: Silica fume powder (Henan Superior Abrasives 2024).

A denser concrete matrix is desirable for several reasons. Denser concrete is generally less permeable because voids in the concrete matrix are fewer and smaller (Chia and Zhang 2002, Galishnikova et al. 2020, Jankovic et al. 2014, Yusuf 2019); in one study, the void percentage of fresh concrete without silica fume ranged from 16 to 20 percent, while the void percentage of concrete containing 10 percent silica fume, as a replacement of portland cement, ranged from 6 to 14 percent. A related benefit is the reduced likelihood of damage from water freezing and expanding inside the concrete (Jankovic et al. 2014, Karakurt and Bayazit 2015); in particular, one study showed that the mass loss of concrete comprising silica fume was nearly half of the mass loss of concretes without silica fume in freeze-thaw cycles (Jankovic et al. 2014). In addition, other deleterious agents, such as chloride ions, are less able to penetrate concrete comprising silica fume (Camarini and Bardella 2013, King 2012, Wolsiefer 1991); chloride penetration depths were observed to be up to 50 percent shallower in concretes comprising silica fume than in concretes without silica fume in one study involving a 90-day test period (Camarini and Bardella 2013).

Concrete comprising silica fume typically exhibits greater 28-day compressive strength (Gong et al. 2020) than concrete without silica fume because of the increased density of the interfacial transition zone, or the zone between individual aggregate particles and the surrounding cementitious paste (Galishnikova et al. 2020); as an example, concrete with 15 percent silica fume, as a replacement of portland cement, exhibited an average compressive strength that was 21 percent greater at 28 days than that of concrete without silica fume (Gong et al. 2020). A higher ultimate strength develops through the pozzolanic reaction despite a lower initial strength that results from an initially lower amount of C-S-H formed through the cement hydration reaction, assuming that a portion of the cement was replaced with silica fume (Galishnikova et al. 2020). Concrete comprising silica fume also has decreased autogenous shrinkage when compared to concrete without silica fume (Yusuf 2019).

Because of its high surface area, silica fume exhibits a high water demand that can lead to construction concerns. One concern is that a high water demand can reduce the workability, or slump, of concrete comprising silica fume compared to concrete without silica fume, all other factors held constant (Galishnikova et al. 2020). Another concern is that a high water demand can cause a decrease in water bleeding during the concrete curing process (Jankovic et al. 2014, King 2012). Since drying of the concrete surface due to insufficient water bleeding can cause plastic shrinkage cracking of the concrete (Mindess et al. 2003), special construction practices are often required for placement of concrete comprising silica fume. For example, spraying a fine mist of water on the concrete surface, or fogging, and/or placing plastic sheeting or wet coverings such as burlap or canvas on the surface of the newly placed concrete will minimize the occurrence of plastic shrinkage cracking (Leonhardt 1988, Mindess et al. 2003).

2.4 Concrete Deterioration Mechanisms

One of the primary failure mechanisms of reinforced concrete is corrosion of the embedded reinforcing steel. When chloride-induced corrosion occurs, the passive oxide film on the surface of the reinforcing steel is compromised through reactions with chloride ions (Murthi and Sivakumar 2008), usually starting at concentrations between 1.3 and 2.0 lb of chloride per cubic yard of concrete (Roper 2018, Wolsiefer 1991). In this process, an anode and a cathode form on the reinforcing steel, with corrosion products forming at the anode (Hebdon 2020). Because the corrosion products can be up to 10 times larger in volume than the original steel (Hebdon 2020), the corrosion process can cause the development of high tensile stresses within the concrete that lead to cracking, delamination, and decreased structural integrity (Hebdon 2020).

The occurrence of chloride-induced corrosion can be minimized by reducing the permeability of the concrete to chloride ions. For this reason, as mentioned previously, the addition of silica fume can be useful because denser concrete is less permeable and therefore less susceptible to both chloride ion and water ingress (King 2012). Nonetheless, the literature review performed for this research identified only one study documenting these expected benefits of silica fume in concrete over the service life of a structure, and the maximum age of the concrete bridge decks tested in that study was 15 years (Hooton et al. 2003); the decks, which were located in New York and Ohio, were exposed to chloride ions through wintertime applications of deicing salts.

Related to the corrosion of reinforcing steel is the depth of carbonation in concrete. Because carbonation reduces the pH of the concrete, carbonation can compromise the passive oxide film surrounding the reinforcing steel when the carbonation depth approaches the cover depth. Concrete carbonation depth is generally accepted to be proportional to the square root of time (Cho et al. 2016); for example, if the carbonation depth is 0.04 in. in 1-year-old concrete, the depth should be approximately 0.12 in. after 9 years, 0.20 in. after 25 years, and 0.39 in. after 100 years.

In addition to corrosion of embedded reinforcing steel, other causes of deterioration of concrete can include shrinkage, settlement, and environmental conditions (Hebdon 2020). Plastic shrinkage cracking can occur when the concrete is curing if the moisture at the surface of the concrete evaporates faster than it can be replaced by bleed water, and drying shrinkage cracking occurs when water is lost from the cement paste after the concrete has hardened (Hebdon 2020). Settlement cracking can occur when concrete settlement is restrained by reinforcing steel in some areas of the concrete yet unrestrained in adjacent areas without reinforcing steel; the resulting differential settlement causes tensile stresses that frequently lead to cracking (Mindess

et al. 2003, Schmitt and Darwin 1995). Environmental conditions such as temperature, humidity, and precipitation can all affect the rate of shrinkage in concrete and can introduce strains due to differences in the physical properties of concrete; for example, concrete that is cooler in one area and warmer in one area can develop tensile stresses that may lead to cracking (Hebdon 2020). Freeze-thaw cycles are also recognized as a mechanism that can cause cracking in concrete when temperatures below freezing cause water within the concrete to freeze and expand, thus also leading to tensile stresses and potential cracking (Hebdon 2020). For these reasons, engineering properties such as cover depth, modulus of elasticity, electrical impedance, chloride permeability, splitting tensile strength, compressive strength, and carbonation depth can greatly influence the performance of concrete.

2.5 Summary

Silica fume is a co-product of silicon and ferrosilicon metals. Similar to other supplementary cementitious materials such as fly ash, silica fume is a pozzolan that is often added to concrete as a partial replacement of portland cement. Typical replacement percentages range from 5% to 25%, and the resulting pozzolanic reaction densifies and strengthens the concrete matrix by facilitating the formation of additional C-S-H, which is the primary binder in concrete.

Denser concrete is generally less permeable because voids in the concrete matrix are fewer and smaller, which makes deleterious agents, such as chloride ions, less able to penetrate the concrete. Concrete comprising silica fume typically exhibits greater 28-day compressive strength than concrete without silica fume because of the increased density of the interfacial transition zone; this higher ultimate strength develops through the pozzolanic reaction despite a lower initial strength that results from an initially lower amount of C-S-H formed through the cement hydration reaction, assuming that a portion of the cement was replaced with silica fume.

Because of its high surface area, silica fume exhibits a high water demand that can lead to construction concerns. One concern is that a high water demand can reduce the workability, or slump, of concrete comprising silica fume compared to concrete without silica fume, and another concern is that a high water demand can cause a decrease in water bleeding during the concrete curing process. Special construction practices are often required for placement of concrete comprising silica fume, such as fogging or placing wet coverings on the surface of the newly placed concrete.

In addition to chloride-induced corrosion of embedded reinforcing steel, other causes of deterioration of concrete can include shrinkage, settlement, and environmental conditions. Freeze-thaw cycles are also recognized as a mechanism that can cause cracking in concrete.

3 PROCEDURES

3.1 Overview

The objective of this research was addressed through analysis of the Salt Lake City International Airport parking structure, which was constructed in 1991. Although much of the original construction documentation was lost in a building fire several years ago, information about the parking structure was provided by members of the concrete industry who were involved with construction of the parking structure. Construction personnel explained that, although records indicating the exact proportions of the concrete mixture(s) used for the parking structure are no longer available, silica fume was added to the concrete as a slurry and the concrete was cured with wet coverings on the surface. Additionally, the ratio of water to cementitious materials was 0.38, and the percentage of silica fume used as a replacement of portland cement was 7.5% on the entrance ramp, helices, and first, second, and third floors of the parking structure (unpublished structural drawings, MHT Architects, June 1989); silica fume was not added to the concrete used on the ground floor slab (personal communication, J. Hall and R. Higley, March 2021). Though not confirmed, the silica fume that was used in the concrete is believed to have been supplied by Elkem (personal communication, C. Bedford and J. Hall, October 2019). Reinforcing steel bars (#4) were used in the concrete decks of the first, second, and third floors, as well as the helices of the parking structure; no reinforcing steel was used in the ground floor slab (unpublished structural drawings, MHT Architects, June 1989).

At the time of this research, the parking structure had been in service for 29 years. During the winter seasons, vehicles carried deicing salts from the roads into the parking structure, tracking them from the entrance ramp into the first level and then either downward to the ground level or upward to the second and third levels. As a result, exposure to chloride ions may have decreased from the first level to the ground level, from the first level to the second level, and from the second level to the third level. The following sections outline the testing plan and discuss field and laboratory testing methods.

3.2 Testing Plan

Five areas within the parking structure were selected for evaluation. These areas were the ground level, the entrance ramp to the first level, the second level, the third level, and the east helix, which carried upward traffic (no testing was performed on the west helix, which carried downward traffic). Although the ground level contained no silica fume or reinforcing steel (personal communication, J. Hall and R. Higley, March 2021), it was tested for comparison with the other areas. The only test area that was not covered by a higher level or the roof of the parking structure was the entrance ramp, which experienced direct exposure to precipitation, for example.

At each of the five areas except the helix, a rectangular grid was established by painting white dots onto the concrete surface at regular intervals of 10 ft to allow accurate mapping of test

locations. The grids on the ground, first (entrance ramp), second, and third levels were 30 ft by 40 ft, 40 ft by 80 ft, 30 ft by 40 ft, and 30 ft by 30 ft, respectively. Six chloride concentration sampling locations and three coring locations were selected in each of the five areas except for the entrance ramp, where a total of 12 chloride concentration sampling locations and six coring locations were selected. Testing locations on the helix were chosen such that samples were collected from elevations corresponding to each level. Within each area, chloride concentration sampling locations with and without cracks were tested. An exception was the third level, which did not exhibit cracking; therefore, no chloride concentration sampling locations with cracks were tested on the third level. Figure 3-1 provides an aerial view of the parking structure, while Figure 3-2 through Figure 3-10 depict the test areas and defined origins.

3.3 Field Testing

Several field tests were performed to evaluate each of the five areas within the parking structure. The following sections provide brief explanations of these tests, including visual inspection, chain dragging, Schmidt hammer testing, cover depth measurements, chloride concentration sampling, and coring.

3.3.1 Visual Inspection

The primary objective of visual inspection was to document the presence of any concrete distresses, such as cracks, scaling, or spalling, within the structure. In particular, locations of cracking were noted for consideration during chloride concentration sampling. The results of the visual inspection informed selection of the five test areas evaluated in this research.

3.3.2 Chain Dragging

After each test area was selected, chain dragging was performed to locate any subsurface delaminations. As shown in Figure 3-11, this test involved dragging a steel chain back and forth within the full test area, with the operator listening for changes in the acoustic response of the deck. In this test, intact concrete produces a clear ringing sound of higher frequency, while delaminated concrete produces a dull, hollow sound of lower frequency. Because the concrete slab at the ground level did not contain reinforcing steel, it was not expected to exhibit delamination and was therefore not evaluated using chain dragging.

3.3.3 Schmidt Hammer Testing

Schmidt hammer testing was performed at each test location within each test area to estimate the compressive strength of the concrete. A small area at each test location was smoothed with an angle grinder to ensure accurate results. As shown in Figure 3-12, the hammer was consistently held perpendicular to the surface of the concrete, and 10 measurements were recorded at each location. An average Schmidt rebound number was computed for each area to estimate the compressive strength of the concrete. Because the average rebound values were comparatively high, common correlations between Schmidt rebound number and compressive strength of concrete were not applicable. Therefore, other equations were considered for this research. In particular, a correlation presented by Aliabdo and Elmoaty (2012) was used, as it accommodates higher Schmidt rebound numbers and produced estimates of compressive strength similar to those measured on the cores that were tested in this research. The correlation, including a units conversion that was implemented for this research, is shown as Equation 3.1:

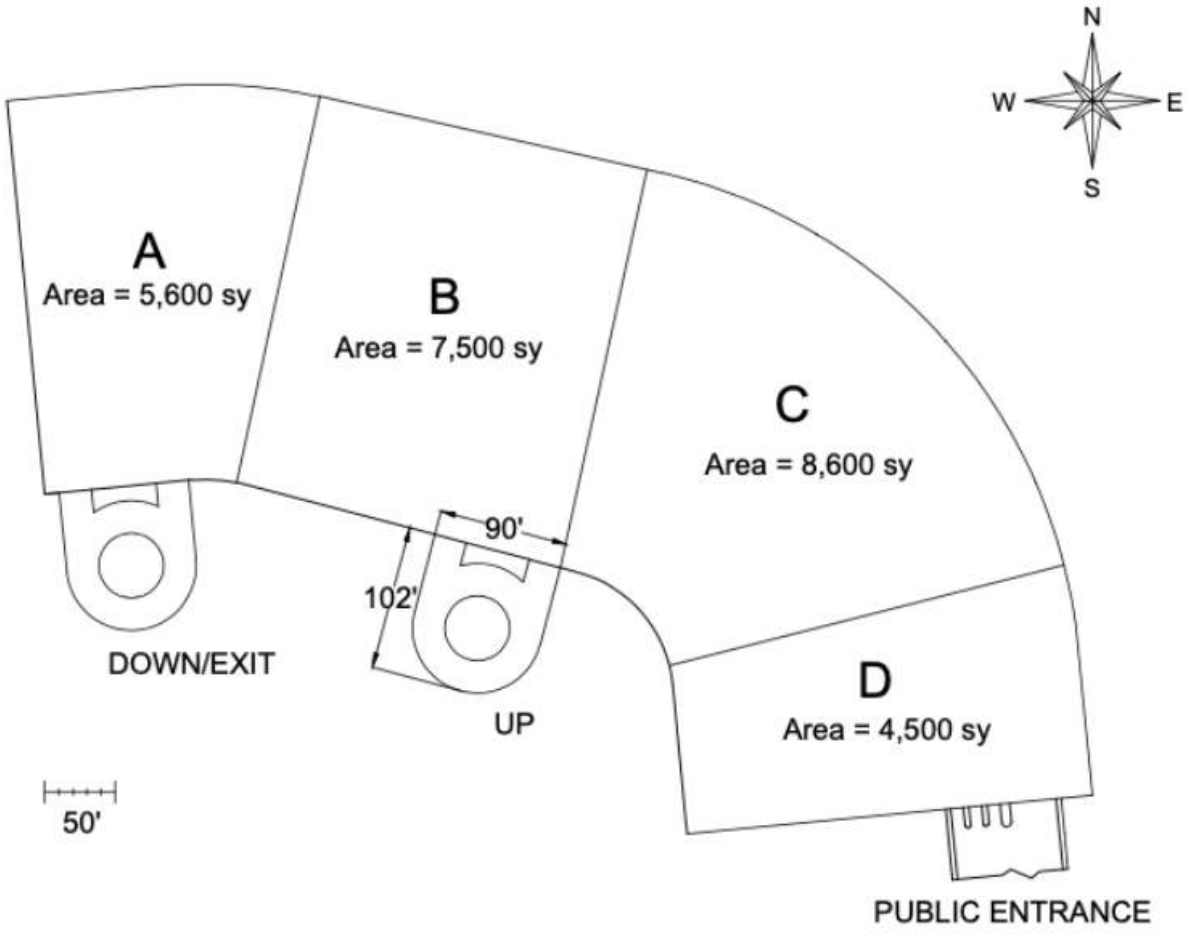

Figure 3-1: Aerial view of parking structure.

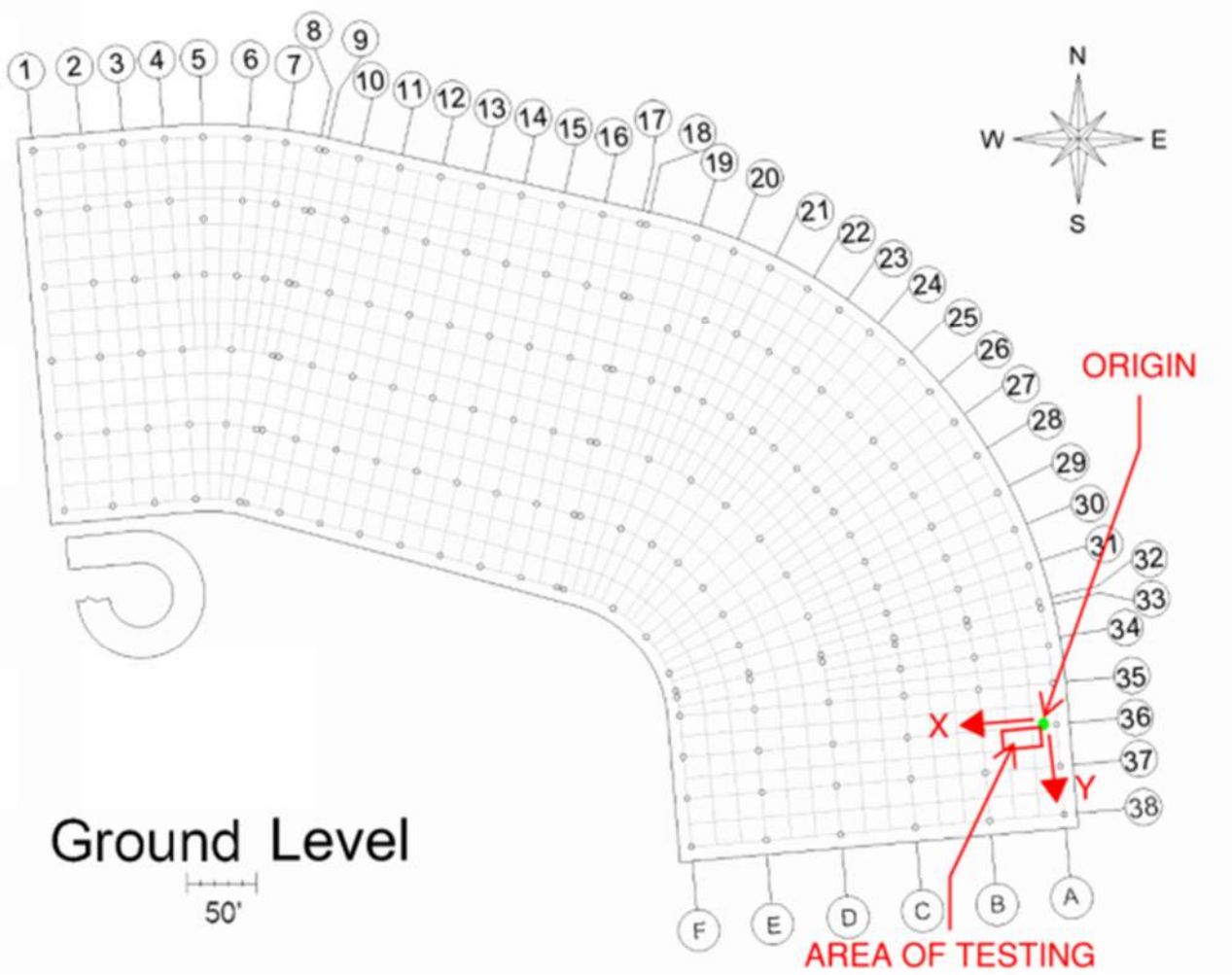

Figure 3-2: Aerial view of ground-level area.

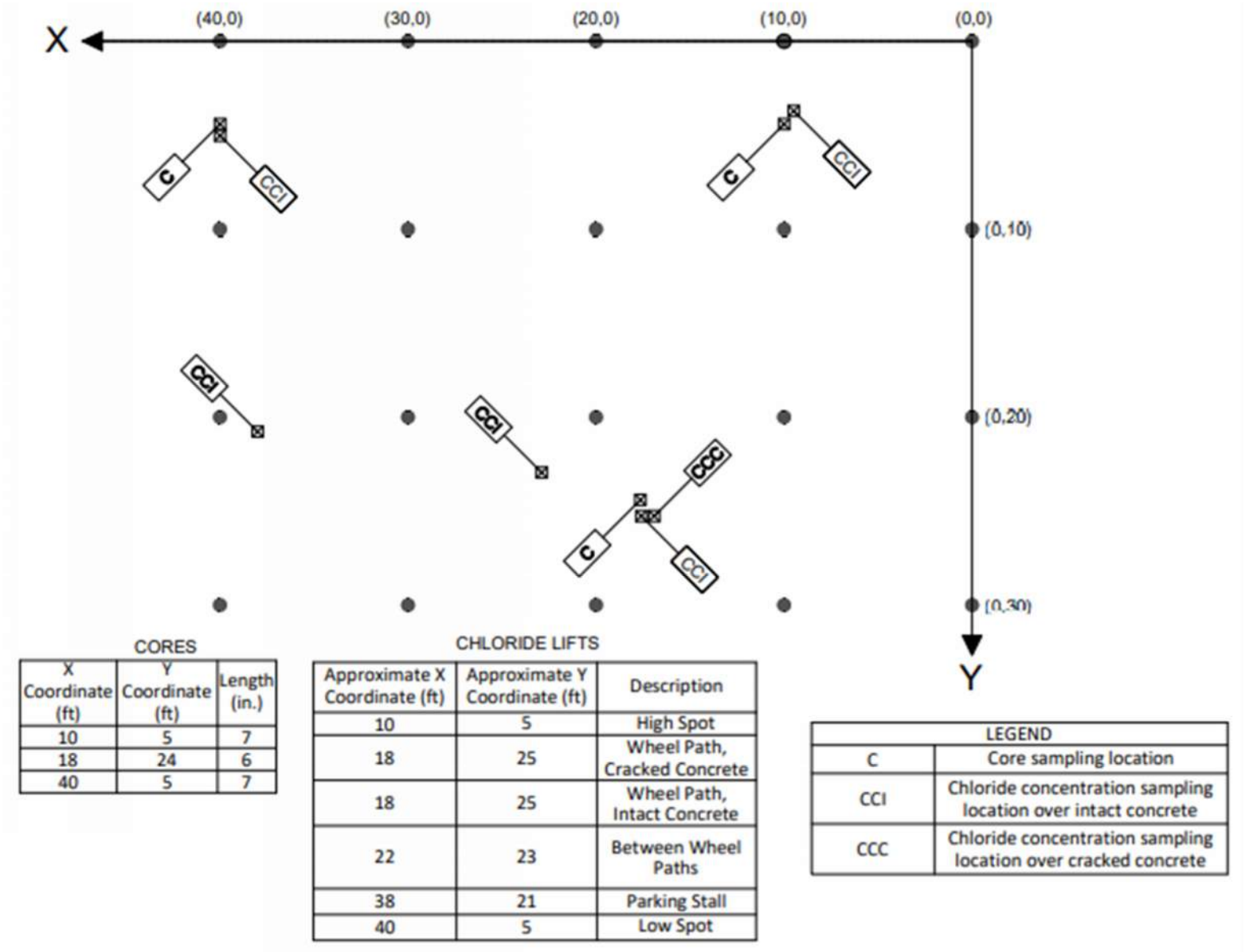

CORES

X Coordinate (ft)	Y Coordinate (ft)	Length (in.)
10	5	7
18	24	6
40	5	7

CHLORIDE LIFTS

Approximate X Coordinate (ft)	Approximate Y Coordinate (ft)	Description
10	5	High Spot
18	25	Wheel Path, Cracked Concrete
18	25	Wheel Path, Intact Concrete
22	23	Between Wheel Paths
38	21	Parking Stall
40	5	Low Spot

LEGEND	
C	Core sampling location
CCI	Chloride concentration sampling location over intact concrete
CCC	Chloride concentration sampling location over cracked concrete

Figure 3-3: Schematic of ground-level area.

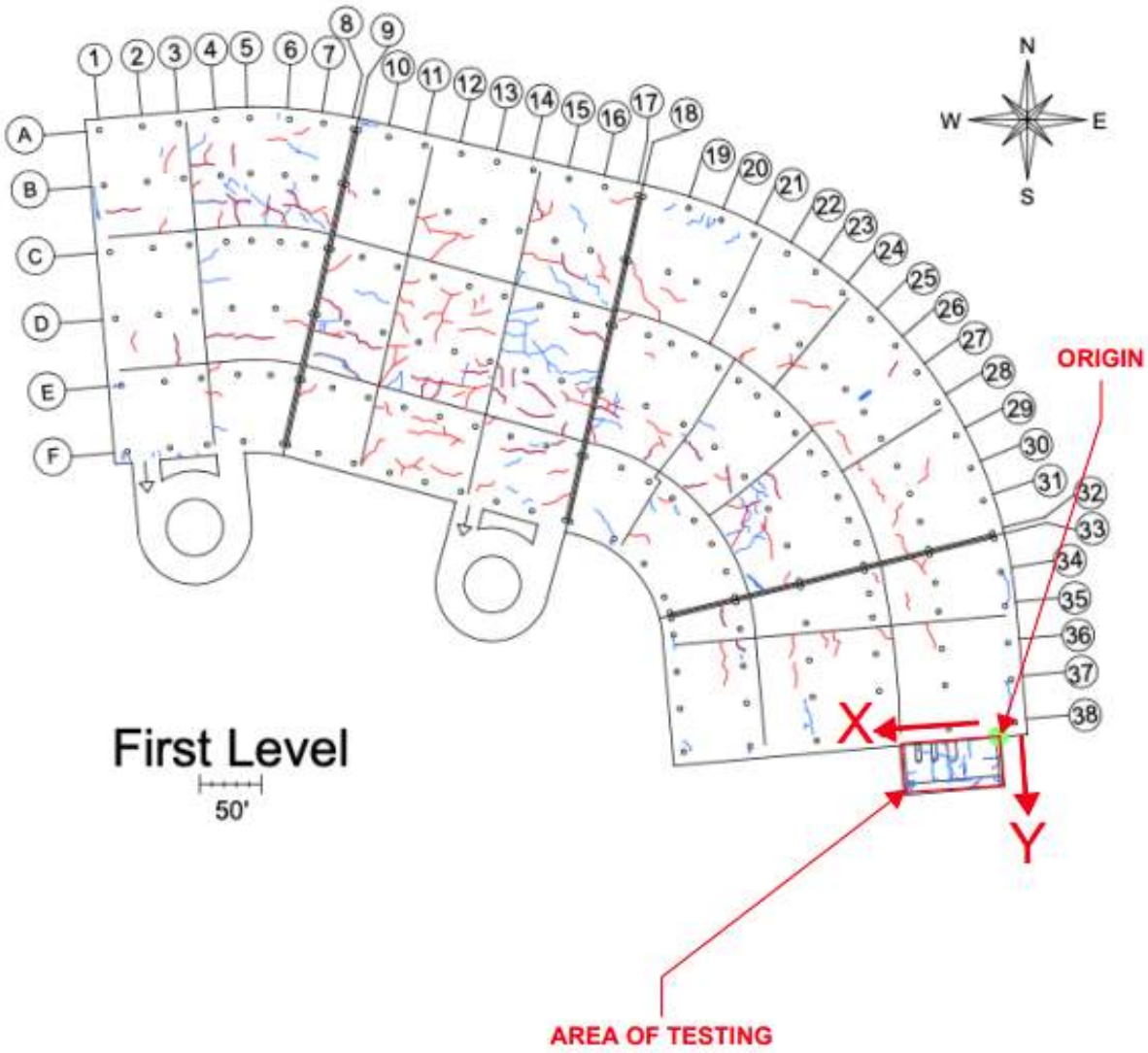

Figure 3-4: Aerial view of entrance-ramp area.

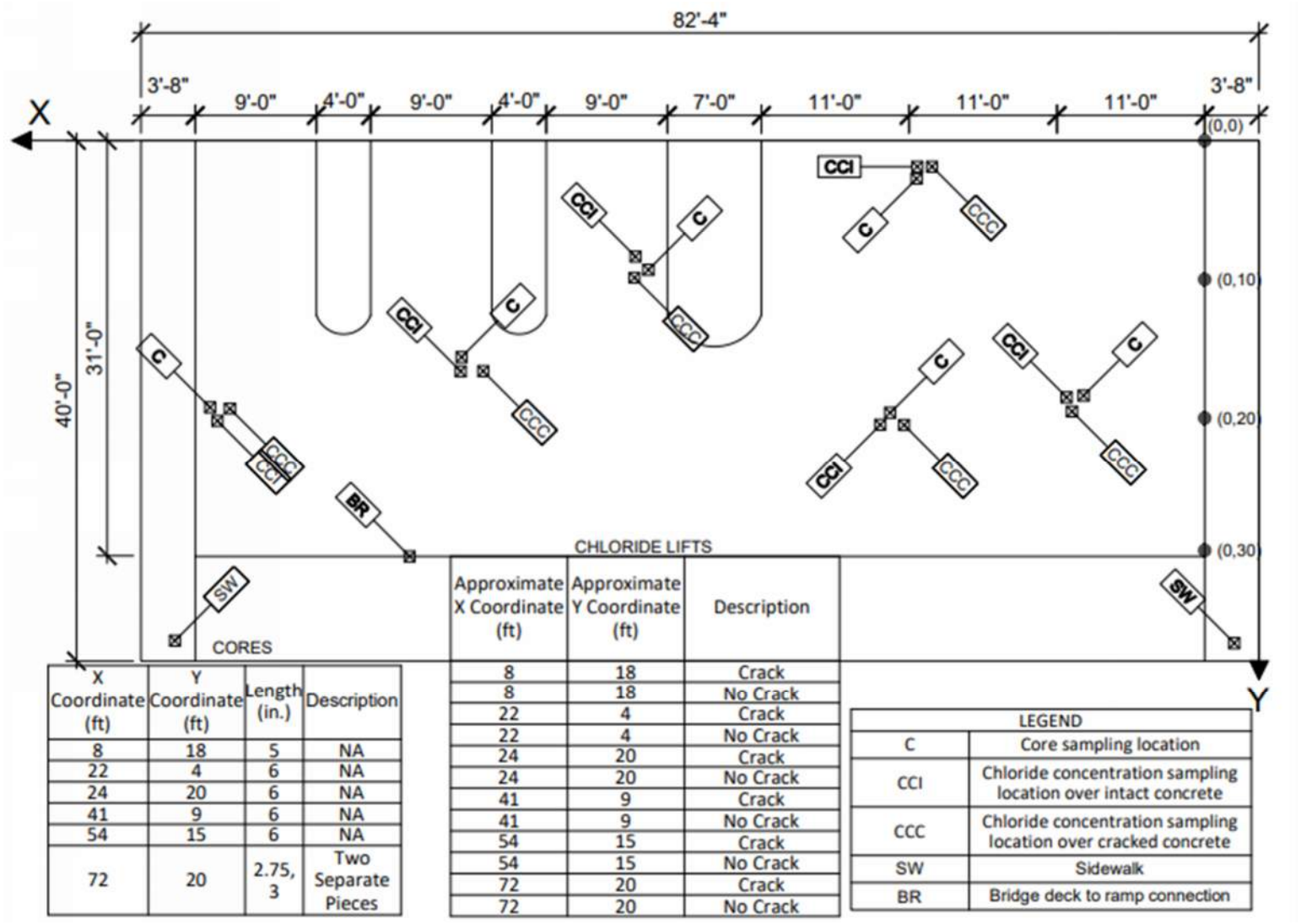

X Coordinate (ft)	Y Coordinate (ft)	Length (in.)	Description
8	18	5	NA
22	4	6	NA
24	20	6	NA
41	9	6	NA
54	15	6	NA
72	20	2.75, 3	Two Separate Pieces

Approximate X Coordinate (ft)	Approximate Y Coordinate (ft)	Description
8	18	Crack
8	18	No Crack
22	4	Crack
22	4	No Crack
24	20	Crack
24	20	No Crack
41	9	Crack
41	9	No Crack
54	15	Crack
54	15	No Crack
72	20	Crack
72	20	No Crack

LEGEND	
C	Core sampling location
CCI	Chloride concentration sampling location over intact concrete
CCC	Chloride concentration sampling location over cracked concrete
SW	Sidewalk
BR	Bridge deck to ramp connection

Figure 3-5: Schematic of entrance-ramp area.

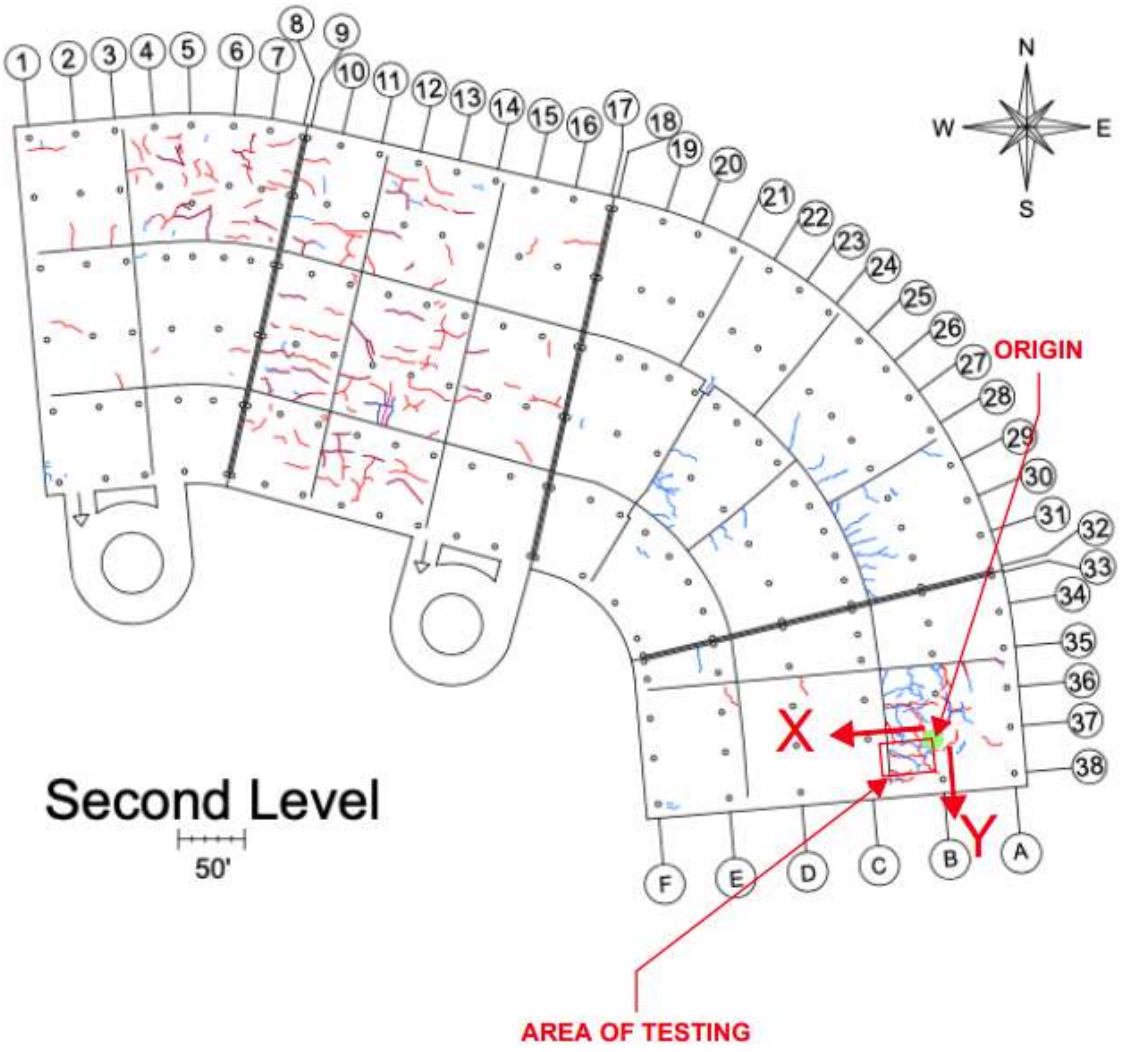

Figure 3-6: Aerial view of second-level area.

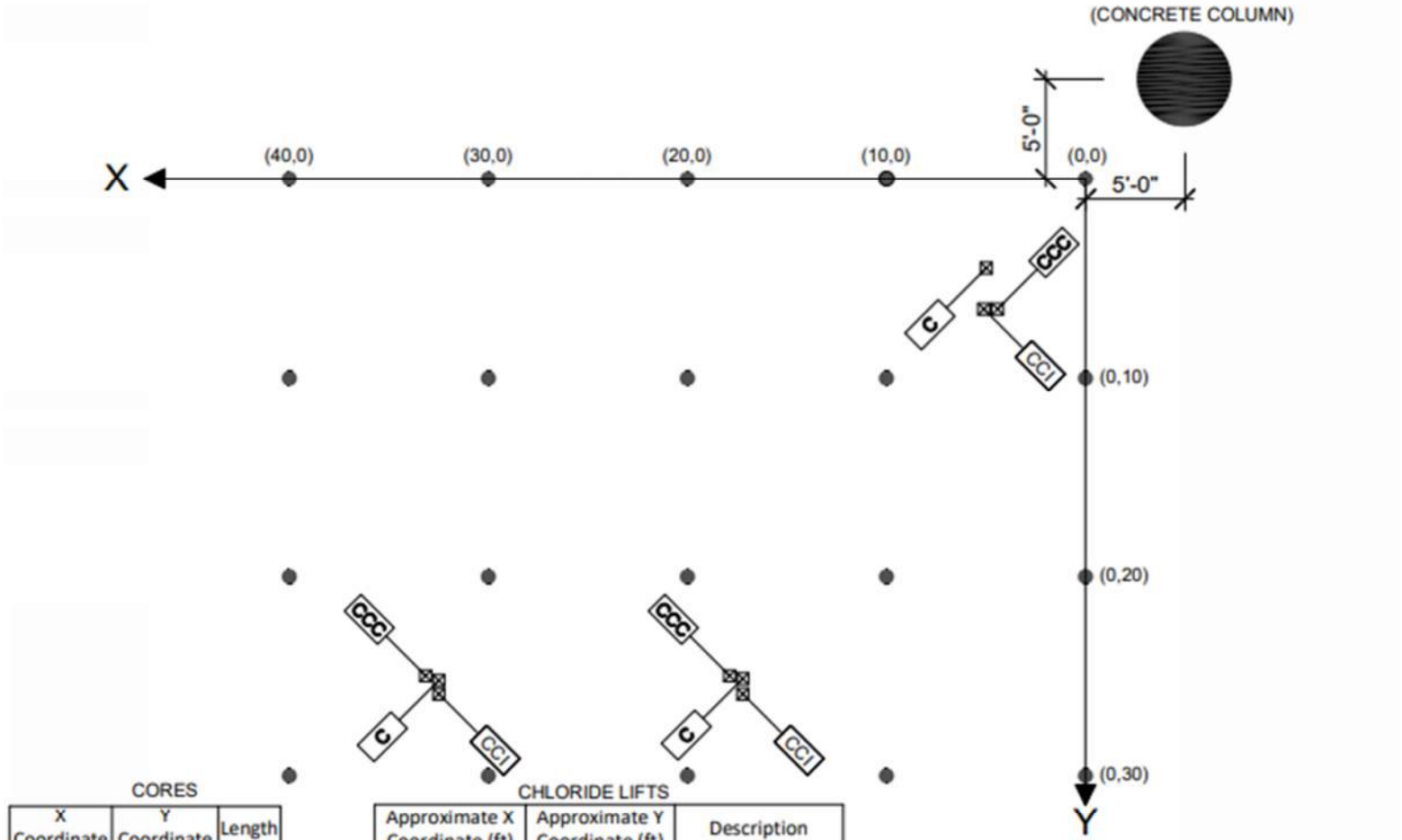

CORES

X Coordinate (ft)	Y Coordinate (ft)	Length (in.)
5	5	9
17	25	8
32	25	7

CHLORIDE LIFTS

Approximate X Coordinate (ft)	Approximate Y Coordinate (ft)	Description
5	7	Crack
5	7	No Crack
18	25	Crack
18	25	No Crack
33	26	Crack
33	26	No Crack

LEGEND	
C	Core sampling location
CCI	Chloride concentration sampling location over intact concrete
CCC	Chloride concentration sampling location over cracked concrete

Figure 3-7: Schematic of second-level area.

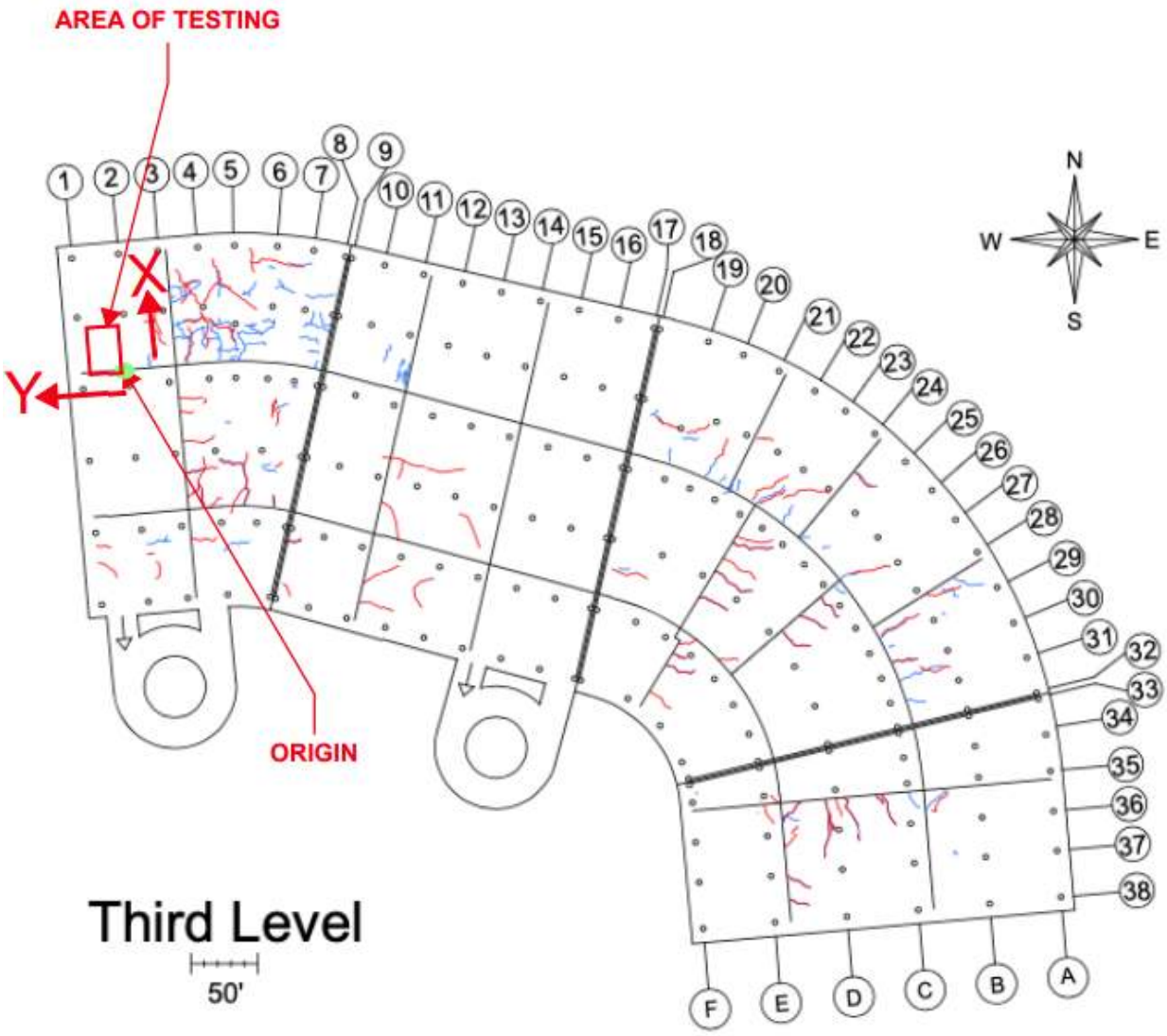

Figure 3-8: Aerial view of third-level area.

CORES

X Coordinate (ft)	Y Coordinate (ft)	Length (in.)	Description
10	10	7	NA
21	20	9	Narrows at one end
31	10	9	NA

CHLORIDE LIFTS

Approximate X Coordinate (ft)	Approximate Y Coordinate (ft)	Description
10	10	NA
10	20	NA
20	10	NA
20	20	NA
30	10	NA
30	20	NA

LEGEND	
C	Core sampling location
CCl	Chloride concentration sampling location over intact concrete

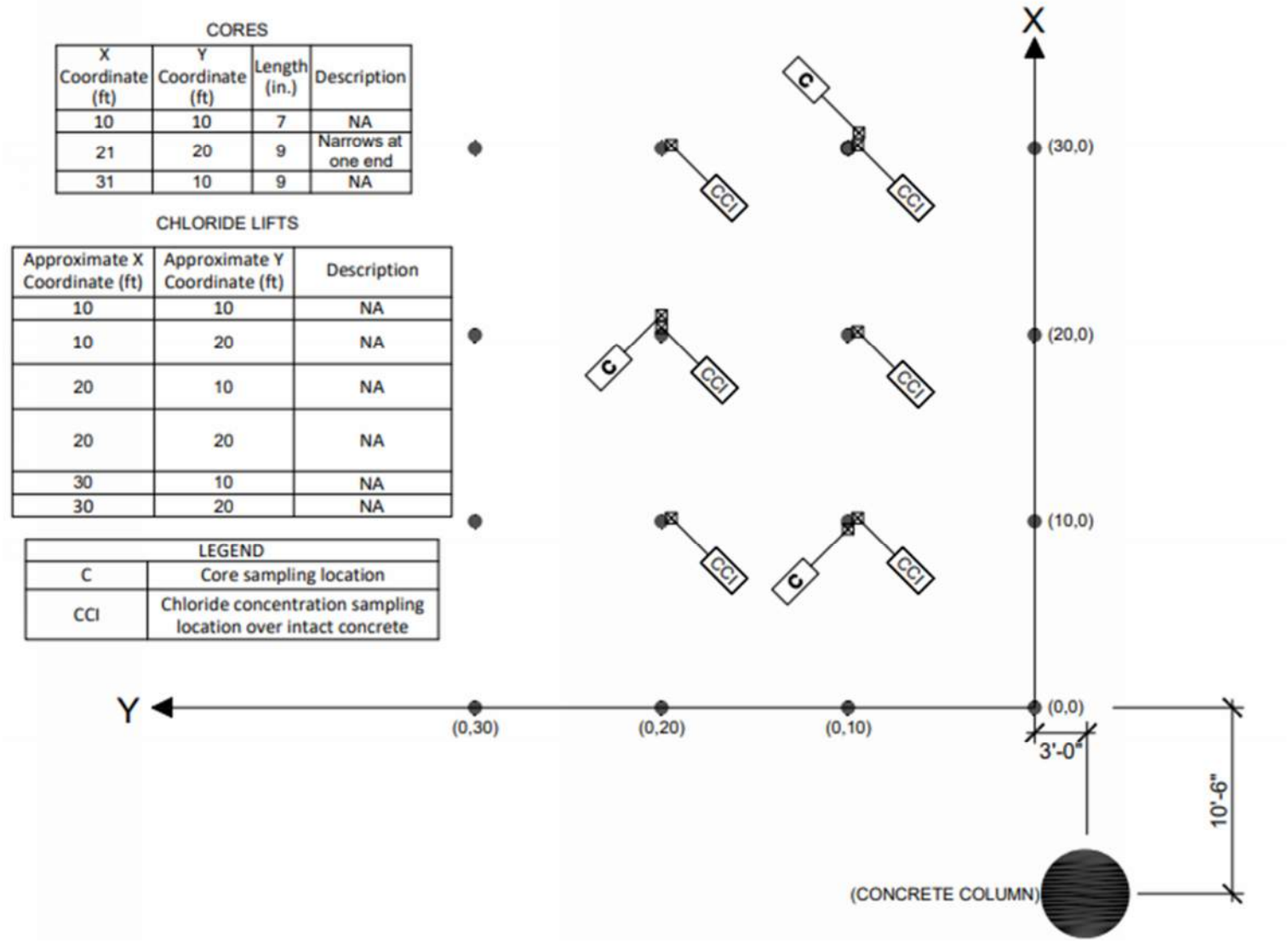

Figure 3-9: Schematic of third-level area.

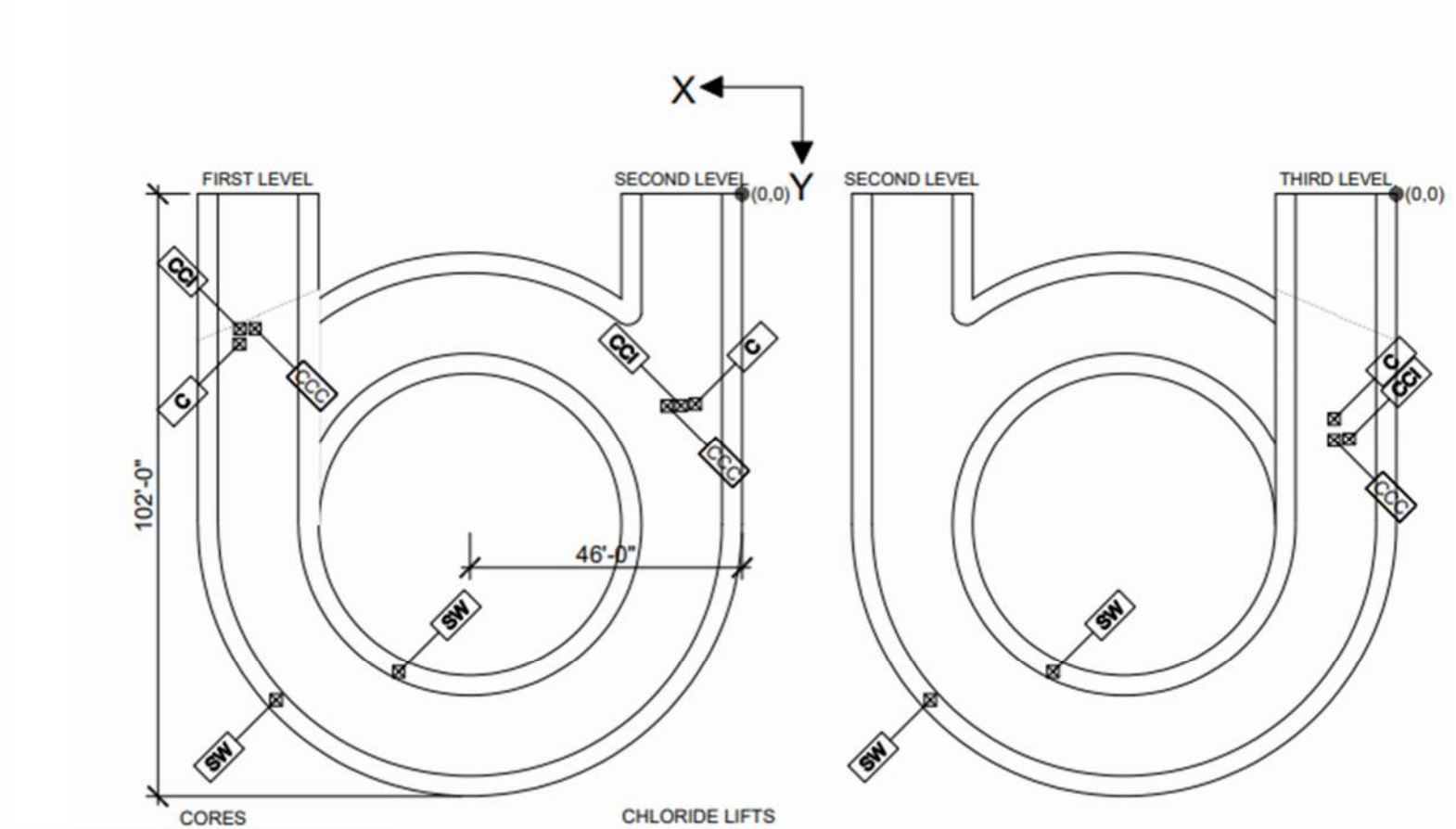

CORES

X Coordinate (ft)	Y Coordinate (ft)	Length (in.)	Description
84	22	3.5	Level 1
12	36	4.25	Level 2
7	41	3	Level 3

CHLORIDE LIFTS

LEVEL	Approximate X Coordinate (ft)	Approximate Y Coordinate (ft)	Description
1	84	22	NA
1	84	22	NA
2	12	36	NA
2	12	36	NA
3	9	41	NA
3	5	41	NA

LEGEND	
C	Core sampling location
CCI	Chloride concentration sampling location over intact concrete
CCC	Chloride concentration sampling location over cracked concrete
SW	Sidewalk

Figure 3-10: Schematic of helix area.

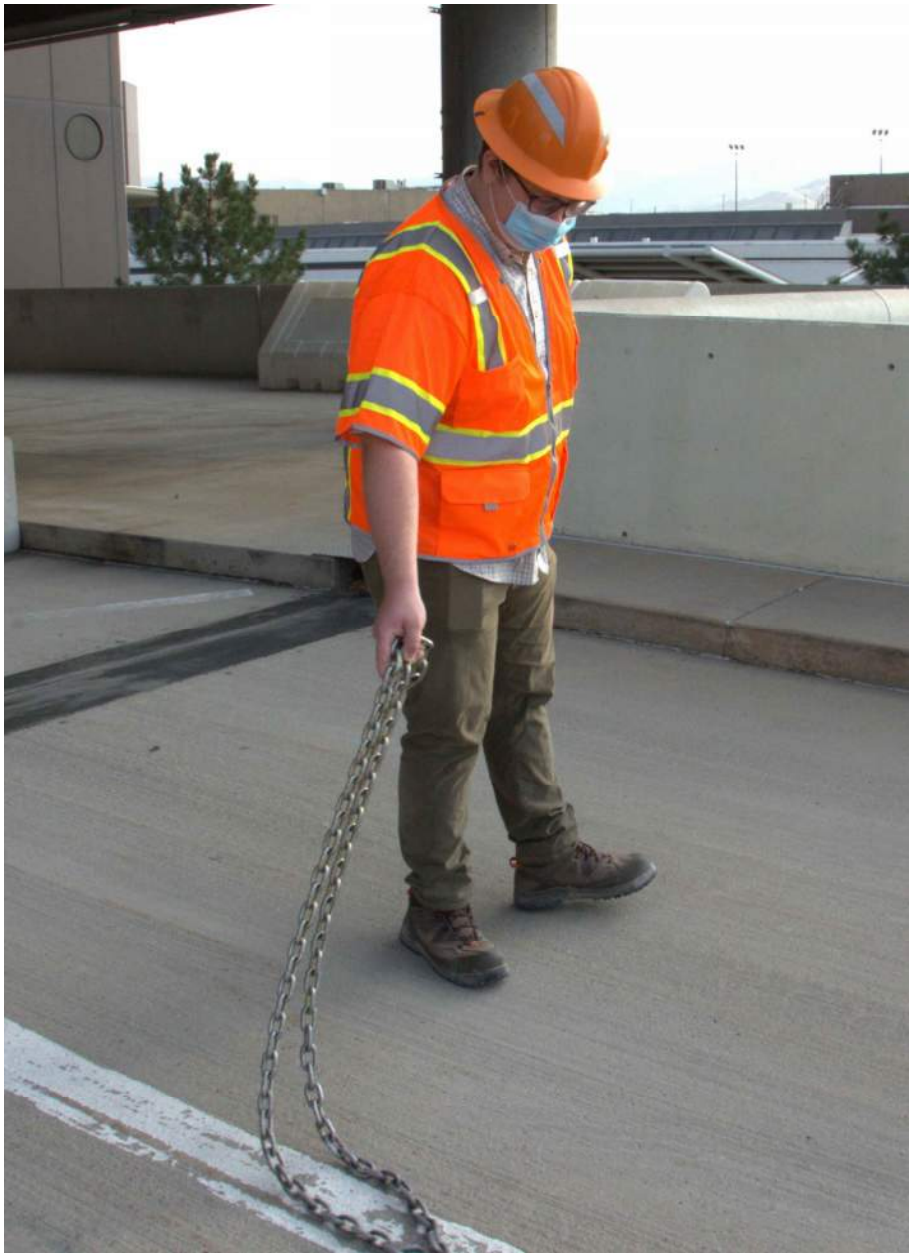

Figure 3-11: Chain dragging.

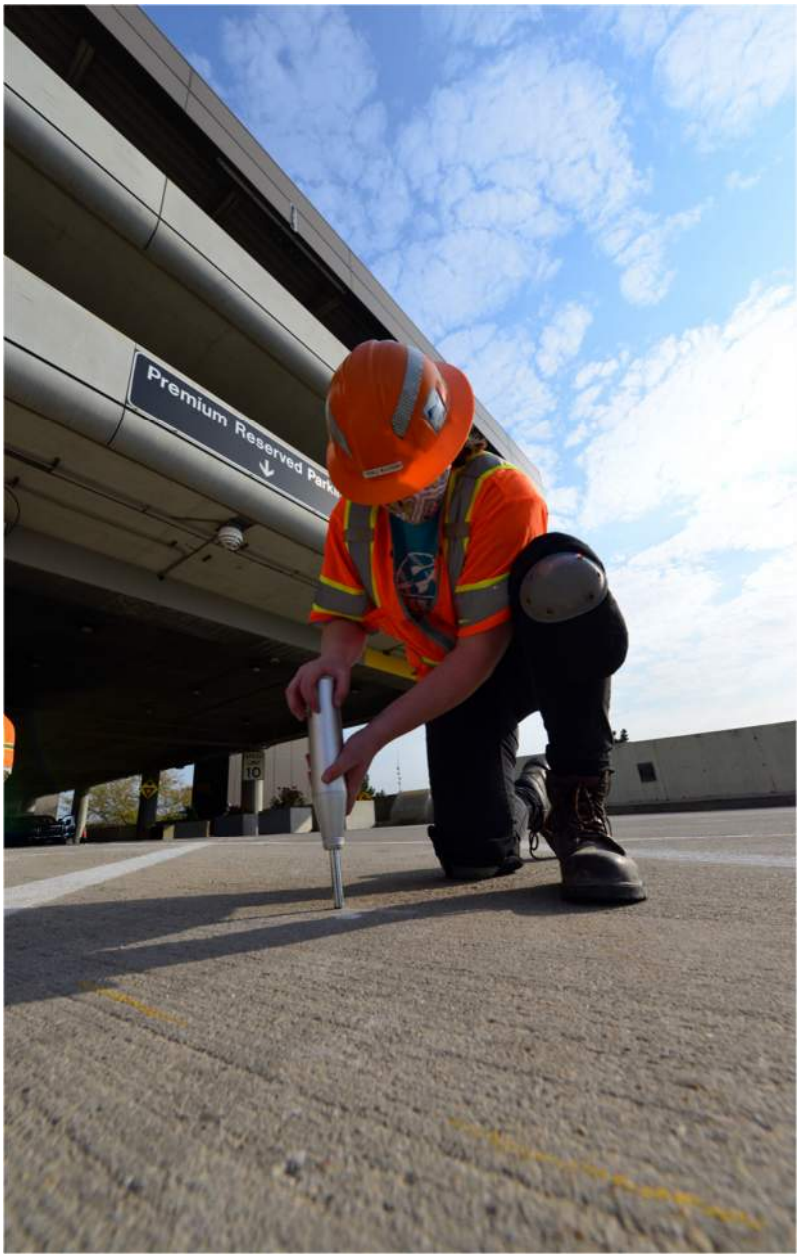

Figure 3-12: Schmidt hammer testing.

$$f_c = (1.933R_n - 51.62)*145.038 \quad (3.1)$$

where

f_c = *compressive strength (psi)*

R_n = *Schmidt rebound number.*

3.3.4 Cover Depth Measurements

Cover depth testing was performed at each test location within each test area, except for the ground level, to locate and estimate the depth of reinforcing steel within the concrete. As previously explained, the ground level was not tested because the concrete slab, which was placed on grade, did not contain reinforcing steel. Figure 3-13 shows the instrument used for

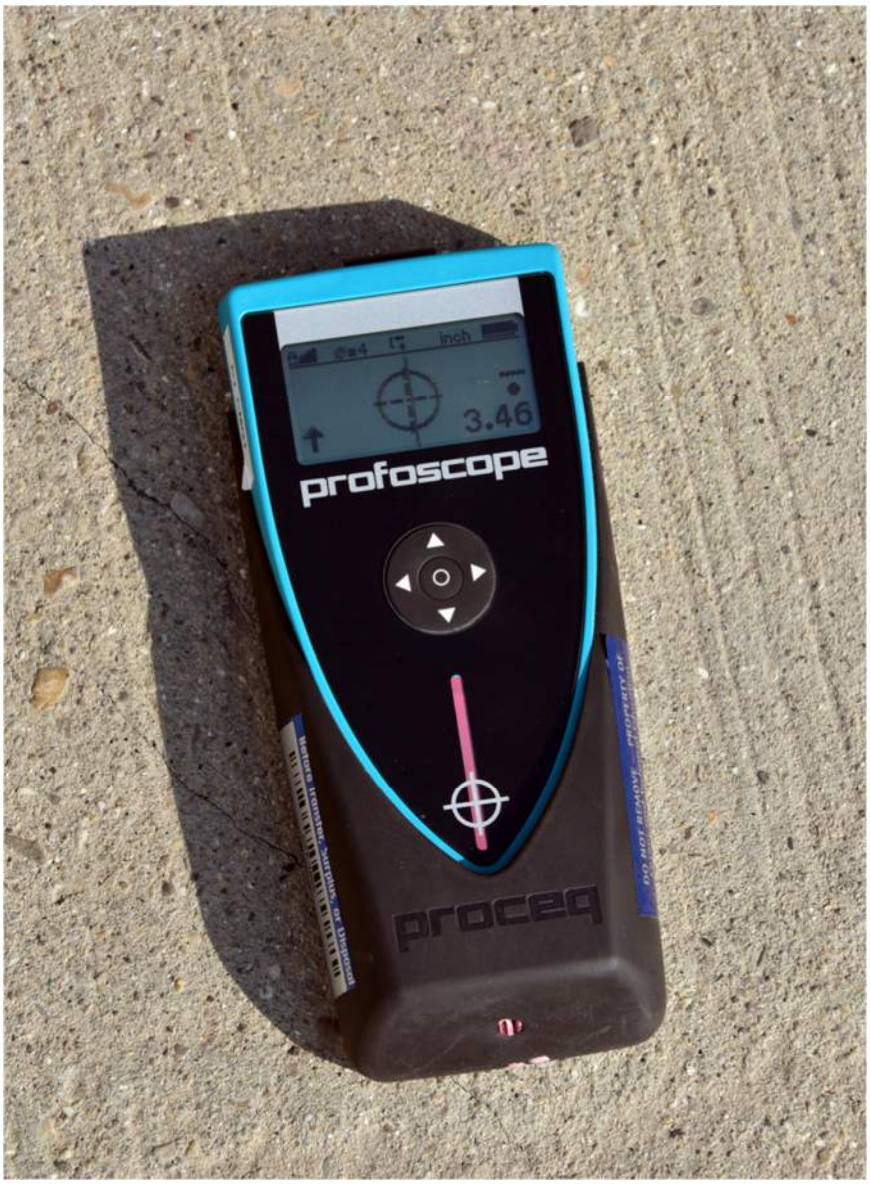

Figure 3-13: Cover depth testing.

testing and an example reading; a minimum of three readings were recorded in each of the test areas. The readings indicate the distance in inches from the surface of the concrete to the top of the nearest reinforcing steel embedded within the concrete. The locations of the reinforcing steel were marked so that chloride concentration sampling and coring could be performed between the bars.

3.3.5 Chloride Concentration Sampling

Chloride concentration sampling was performed within each test area to obtain concrete powder necessary for determining chloride concentration profiles within the concrete. As shown in Figure 3-14, a drill bit was consistently held perpendicular to the concrete, and six locations were sampled within each testing area except for the entrance ramp, where 12 locations were sampled.

At each test location, concrete powder samples were obtained in four to seven lifts that were each approximately 1 in. deep. Seven different hammer drill bits ranging in size from 1.75 in. to 0.875 in. in diameter were used, as listed in Table 3-1. The drill bit diameter decreased with increasing depth to minimize contamination of deeper samples by reducing the probability that near-surface concrete would be inadvertently scraped during the drilling process. A schematic showing the sequential reductions in bit diameter with increasing depth is presented in Figure 3-15.

Figure 3-14: Chloride concentration sampling.

Table 3-1: Chloride Sampling Lift and Drill Bit Diameter

Lift	Drill Bit Diameter (in.)
1	1.75
2	1.5
3	1.375
4	1.25
5	1.125
6	1
7	0.875

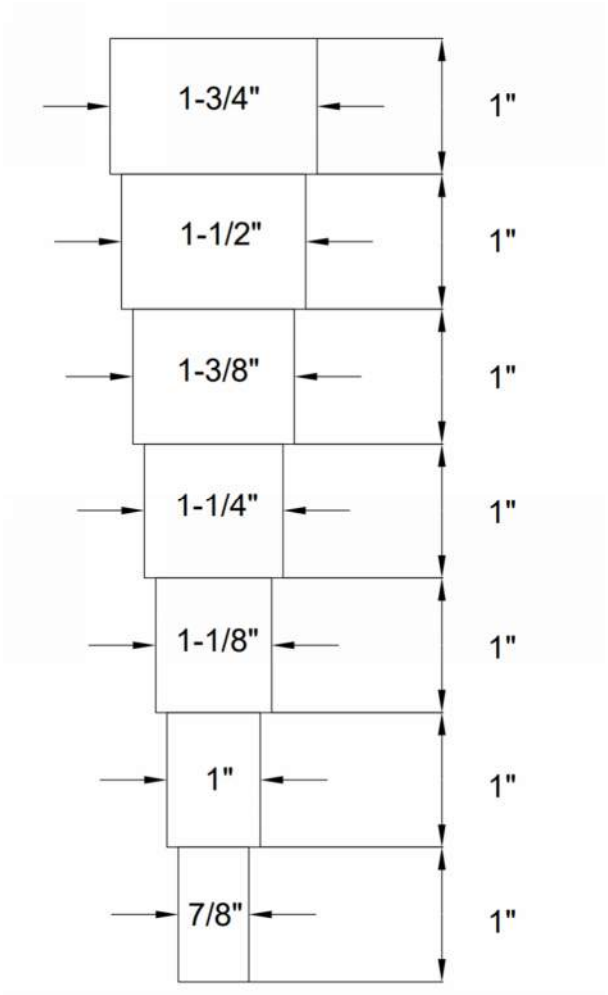

Figure 3-15: Hole dimensions for chloride concentration sampling.

After each lift was drilled, the pulverized concrete powder was removed from the hole with a sampling spoon and placed into a plastic bag. The hole, drill bit, and spoon were then cleaned using compressed air, a small brush, and a vacuum, and the depth of the hole was measured using a ruler before the next lift was drilled. Upon completion of the field testing, the pulverized concrete samples were transported to the Brigham Young University (BYU) Highway Materials Laboratory for analysis.

3.3.6 Coring

Coring was performed within each test area to obtain samples of intact concrete for additional laboratory testing. A truck-mounted coring machine equipped with a 4-in.-diameter core bit was used, and the coring depth was limited to a depth shallower than the deck thickness to prevent loss of the core below the deck. Three cores were obtained from each area, except for the entrance ramp where six cores were obtained. Table 3-2 shows the label given to each core for tracking throughout the testing process, the location with respect to the origin defined within the grid on each level as shown in Figure 3-2 to Figure 3-10, and the laboratory tests subsequently performed on each core.

3.4 Laboratory Testing

Concrete samples were removed from a total of 19 coring locations and 36 chloride concentration sampling locations within the parking structure for additional testing in the BYU Highway Materials Laboratory. Before testing, the lower end of each concrete core was initially trimmed with a masonry saw so that both circular end faces were flat and parallel to each other. The weight and average height of each core were then measured. Non-destructive tests, including modulus of elasticity and electrical impedance, were then performed on all concrete cores prior to destructive tests, which were performed strategically based on the length of the cores and after additional cutting was completed, as shown in Figure 3-16.

The following sections describe the various non-destructive and destructive tests, including chloride concentration, impact resonance, electrical impedance, rapid chloride permeability, splitting tensile strength, compressive strength, and carbonation depth tests, that were performed in the laboratory.

3.4.1 Chloride Concentration Testing

Chloride concentration testing was performed on the samples collected in the field to estimate the concentration of chlorides in general accordance with ASTM C1152 (Standard Test Method for Acid-Soluble Chloride in Mortar and Concrete). Because a rotary hammer was used for sample removal, the samples were sufficiently pulverized to pass the No. 50 (0.0018-in.) sieve, as required, without additional processing. Following oven-drying and digestion, a portion of each sample was titrated, and the chloride concentration was recorded as a percentage of the mass of the sample and then converted to pounds per cubic yard of concrete based on a typically assumed concrete unit weight of 145 lb/yd^3.

3.4.2 Modulus of Elasticity Testing

Impact resonance was performed on each concrete core to estimate the modulus of elasticity of the concrete. As shown in Figure 3-17, the core was supported on two foam pads to acoustically isolate it from the bench during testing. An accelerometer was attached to one end of the core, and a hammer instrumented with a load cell was then used to lightly tap the opposite end of the core. The impact from the hammer caused stress waves to resonate within the concrete, as

Table 3-2: Core Designation, Location, and Tests

Core Identification Number	Level	Coordinate (ft)		Tests Performed					
		X	Y	Impact Resonance	Electrical Impedance	RCPT	Splitting Tensile Strength	Compressive Strength	Carbonation Depth
G 10-5	Ground	10	5	X	X			X	X
G 18-24	Ground	18	24	X	X		X		X
G 40-5	Ground	40	5	X	X	X			
Lane 1	Ramp	8	17.5	X	X		X		X
Lane 2	Ramp	22	3.5	X	X			X	X
Lane 3	Ramp	24	20	X	X	X			
Lane 4	Ramp	41	9	X	X	X			
Lane 5	Ramp	54.25	15	X	X			X	X
Lane 6 (Top)	Ramp	72	19.5	X	X		X		X
Lane 6 (Bottom)	Ramp	72	19.5	X	X		X		X
L2 5-5	2	5	5	X	X			X	X
L2 17-25	2	17	25	X	X	X			
L2 32-25	2	32	25	X	X		X		X
L3 10-10	3	10	10	X	X		X		X
L3 21-20	3	21	20	X	X	X			
L3 30.5-9.5	3	30.5	9.5	X	X			X	X
Helix L1	Helix Level 1	84	22	X	X	X			
Helix L2	Helix Level 2	12	36	X	X			X	X
Helix L3	Helix Level 3	7	41	X	X		X		X

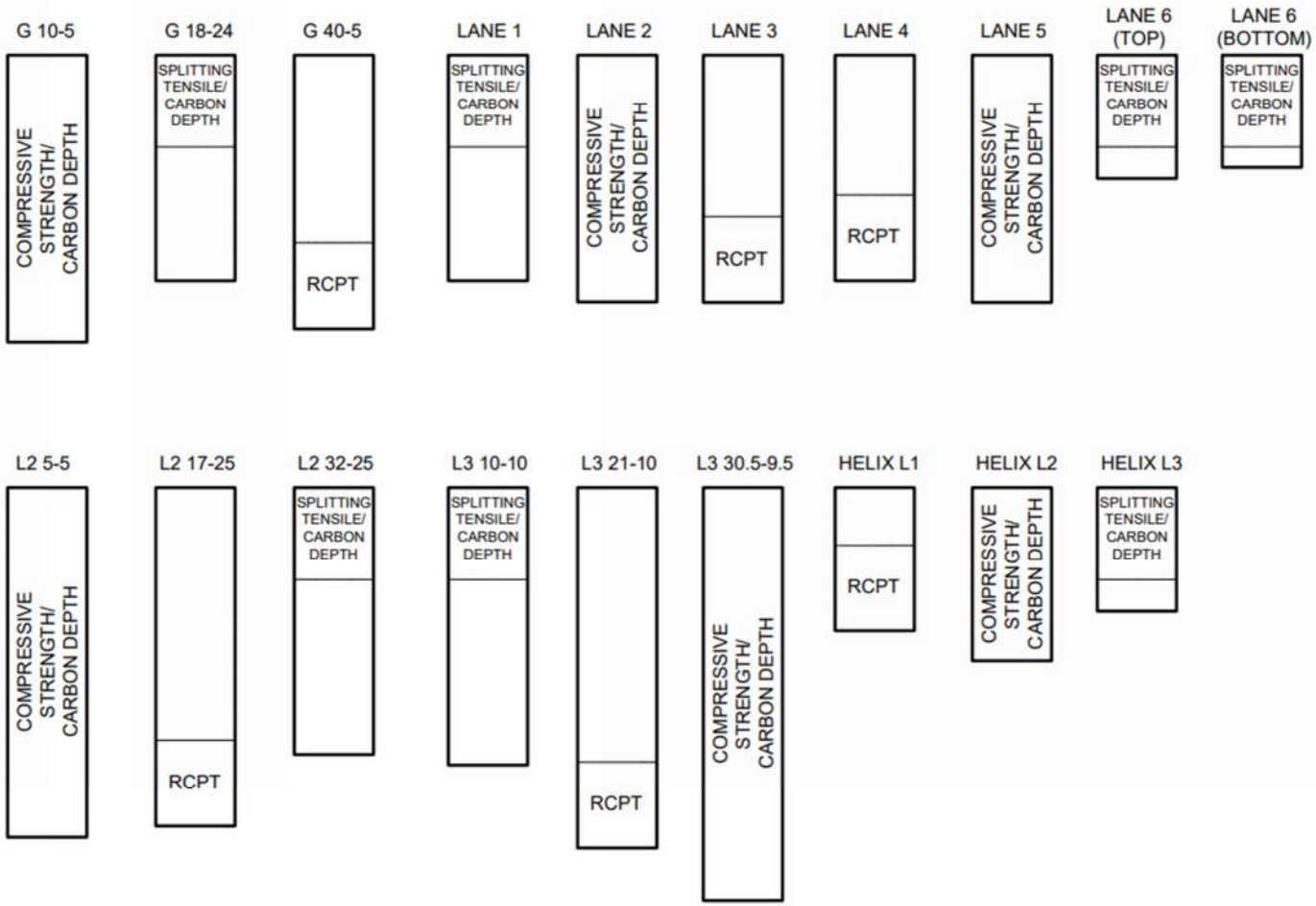

Figure 3-16: Concrete samples.

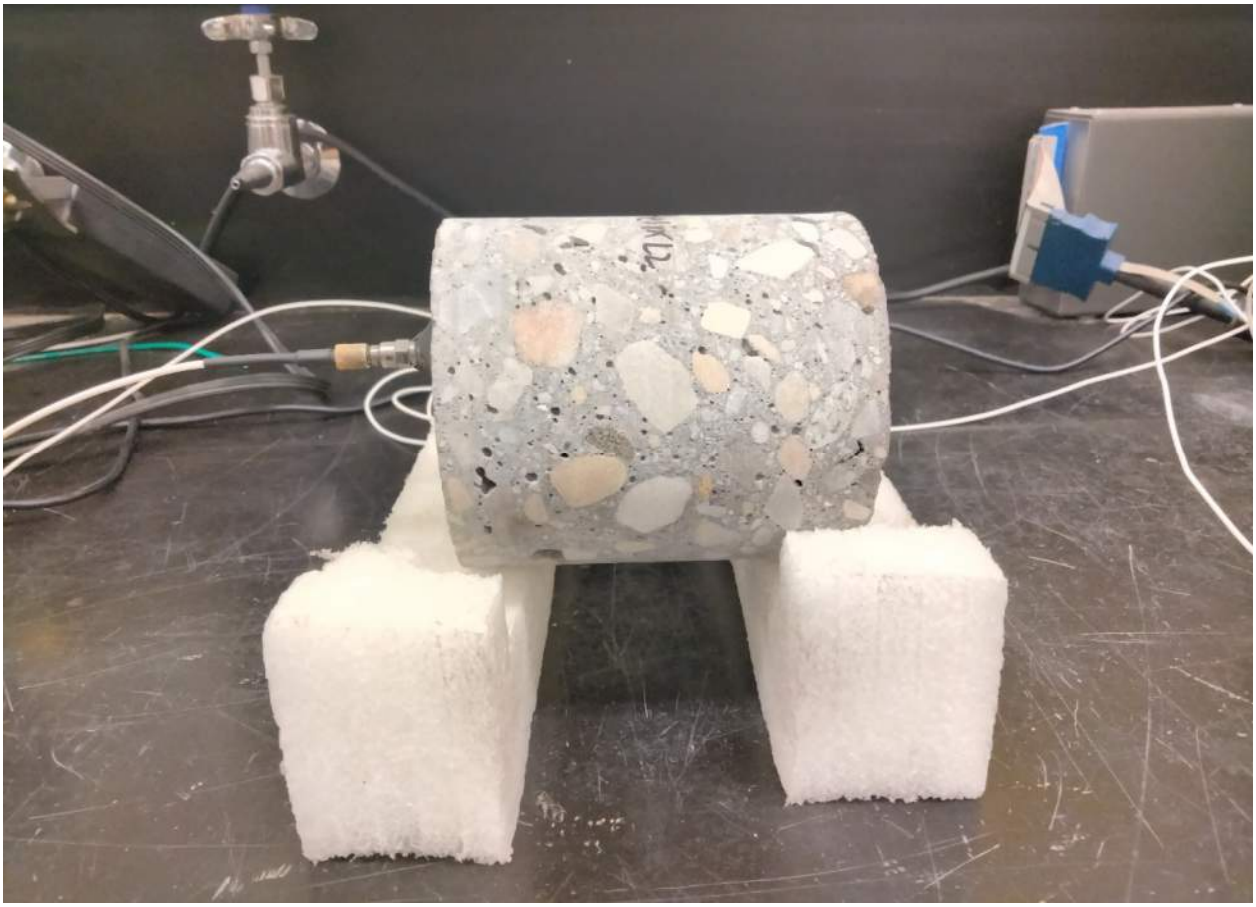

Figure 3-17: Impact resonance testing.

measured by the accelerometer, and the resonant frequency in hertz and the modulus of elasticity in kips per square inch were then determined for each core. Equation 3.2 was used to estimate the modulus of elasticity:

$$E = \frac{\gamma}{32.2} * (2 * l * f)^2 * \frac{1}{144} \quad (3.2)$$

where

E = Young's modulus (psi)

γ = density of the specimen (pcf)

l = length of the specimen (ft)

f = resonant frequency of the specimen (Hz).

3.4.3 Electrical Impedance Testing

Electrical impedance testing was performed on each core to estimate the resistivity of the concrete. As shown in Figure 3-18, each core was positioned horizontally between two vertically-oriented electrodes through which an alternating electrical current was passed for an average of 5 minutes. The average resistance of each specimen was recorded by averaging the measured ohms from all data points when the frequency was approximately 200 Hz. Equation 3.3 was used to normalize the electrical impedance by core length:

$$Rn = R / L \quad (3.3)$$

where

Rn = electrical impedance normalized by core length (ohms/in.)

R = electrical impedance (ohms)

L = core length (in.).

3.4.4 Rapid Chloride Permeability Testing

RCPT was performed on six of the cores to estimate the chloride permeability, or resistance to chloride ion penetration, of the concrete in general accordance with ASTM C1202 (Standard Test Method for Electrical Indication of Concrete's Ability to Resist Chloride Ion Penetration). For this testing, a 2-in.-thick disk was trimmed from the bottom of each core, where previous exposure to chloride ions was expected to be minimal, for evaluation in this test. Each disk was vacuum-saturated with deaired, deionized water prior to being placed in an RCPT cell as shown in Figure 3-19. Each cell was then connected to a controller, and testing was performed at 60V for 6 hours. The chloride permeability in coulombs was recorded for each test.

3.4.5 Splitting Tensile Strength Testing

Splitting tensile strength testing was performed in general accordance with ASTM C496 (Standard Test Method for Splitting Tensile Strength of Cylindrical Concrete Specimens) to estimate the tensile strength of the concrete. When possible, specimens were cut to approximately 2.5 in. in length. Two of the core specimens, core "Helix L3" and "Lane 6 Top," were less than 3 in. and were not cut to 2.5 in. because the saw was not equipped to clamp such short specimens. Prior to testing, the height, weight, and diameter of each specimen were

Figure 3-18: Electrical impedance testing.

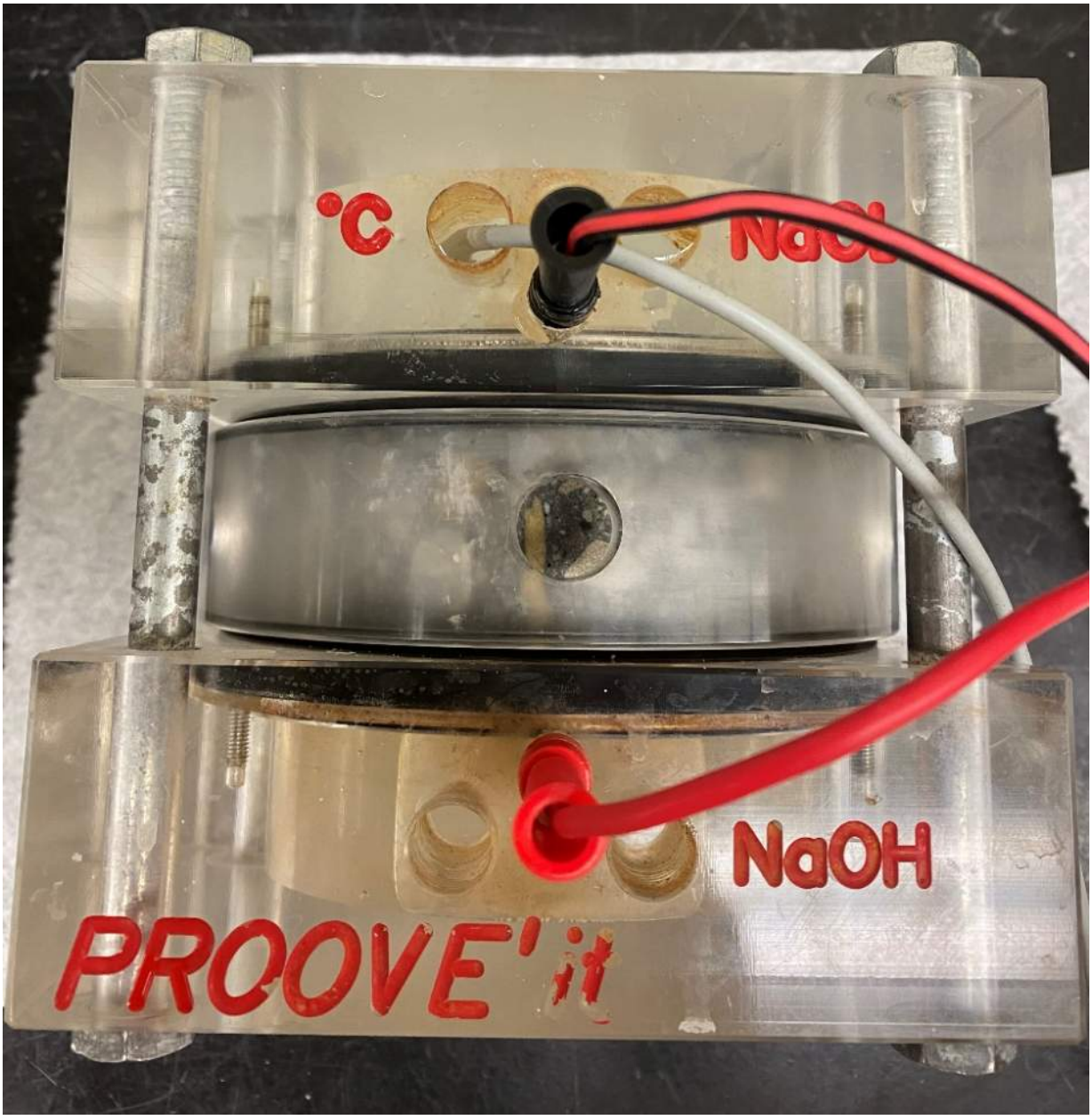

Figure 3-19: Rapid chloride permeability testing.

recorded, and two diametrically opposed locations on sides with the least amount of observable defects, such as voids, were marked with a line on the specimen to indicate the desired points of contact with the upper and lower platens. Thin strips of softwood, approximately 0.125 in. thick, were placed between the specimen and the platens, as shown in Figure 3-20. Each specimen was tested at a target strain rate of 0.05 in./minute, and the peak load in pounds was recorded. Equation 3.4 was used to calculate the splitting tensile strength of the specimens:

$$T = 2 * P / (\pi * L * D) \quad (3.4)$$

where

T = splitting tensile strength (psi)
P = maximum load (lbs)
L = core length (in.)
D = core diameter (in.).

3.4.6 Compressive Strength Testing

Compressive strength testing was performed in general accordance with ASTM C39 (Standard Test Methods for Compressive Strength of Cylindrical Concrete Specimens) to estimate the compressive strength of the concrete. Prior to the testing, the weight, length, and diameter of each specimen were recorded. As shown in Figure 3-21, each specimen was capped with sulfur and tested at a target strain rate of 0.05 in./minute, and the peak load in pounds was recorded. Equation 3.5 was used to calculate the compressive strength of each specimen:

$$C = P / (\frac{\pi * D^2}{4}) \quad (3.5)$$

where

C = compressive strength (psi)
P = maximum load (lbs)
D = core diameter (in.).

3.4.7 Carbonation Depth Measurements

Carbonation depth testing was performed on each of the cores that were previously subjected to splitting tensile strength testing and compressive strength testing to estimate the depth of carbonation in the concrete. Immediately after failure in either the splitting tensile strength or compressive strength test, a solution of phenolphthalein indicator was sprayed onto a middle portion of both sides of a failure surface at the upper end of the core, corresponding to the top of the concrete deck, and the maximum depth of carbonation on each side was recorded. As shown in Figure 3-22, the concrete that did not experience carbonation turned pink, indicating a pH greater than about 9, while the concrete that did experience carbonation remained colorless, indicating a pH less than about 9. The maximum apparent depth of carbonation in inches was measured at these colorless sections.

Figure 3-20: Splitting tensile strength testing.

Figure 3-21: Compressive strength testing.

Figure 3-22: Carbonation depth testing.

3.5 Summary

The objective of this research was addressed through analysis of the Salt Lake City International Airport parking structure. Five areas within the parking structure were selected for evaluation. These areas were the ground level, the entrance ramp to the first level, the second level, the third level, and the east helix. Several field tests were performed to evaluate each of the five areas within the parking structure. These tests included visual inspection, chain dragging, Schmidt hammer testing, cover depth measurements, chloride concentration sampling, and coring. Concrete samples were removed from a total of 19 coring locations and 36 chloride concentration sampling locations within the parking structure for additional testing in the BYU Highway Materials Laboratory. The various non-destructive and destructive tests performed in the laboratory included chloride concentration, impact resonance, electrical impedance, rapid chloride permeability, splitting tensile strength, compressive strength, and carbonation depth tests.

4 TEST RESULTS

4.1 Overview

The following sections present the results of the field and laboratory testing performed for this research. While some potentially confounding variables, including but not limited to construction practices, drainage, or exposure of the concrete, may have influenced the properties and performance of the concrete together with the mixture design details, evaluating the effects of these variables was not within the scope of this study.

4.2 Field Testing Results

The results of visual inspection, chain dragging, Schmidt hammer testing, and cover depth measurements are presented in the following sections.

4.2.1 Visual Inspection

The primary purpose of visual inspection was to document the presence of any concrete distresses, such as cracks, scaling, or spalling, within the structure. As documented in a previous report (Bordelon et al. 2021), the average crack density within the parking structure ranged from 0.002 to 0.095 ft/ft^2, and no potholes were observed in any of the decks. No differences were apparent between concrete comprising silica fume and concrete without silica fume.

4.2.2 Chain Dragging

Chain dragging, which was performed only on concrete comprising silica fume, did not identify any delaminations within the test areas.

4.2.3 Schmidt Hammer Testing

Schmidt rebound numbers are shown in Table 4-1 through Table 4-5, and the average values for the ground level, entrance ramp, second level, third level, and helix were 55, 59, 57, 55, and 57, respectively. With the average Schmidt rebound number ranging from 55 to 59 for the test areas, the compressive strengths estimated using Equation 3.1 ranged from 7933 psi to 9159 psi as shown in Table 4-6. The average estimated compressive strengths of concrete comprising silica fume and concrete without silica fume were 8488 psi and 7933 psi, respectively.

4.2.4 Cover Depth Measurements

Cover depth measurements for the entrance ramp, second level, third level, and helix, which were all constructed using concrete comprising silica fume, are shown in Table 4-7 through Table 4-10, respectively. The ground level, which was constructed using concrete without silica fume, was not tested because reinforcing steel was not present at that level. The average depths to the top of the rebar, which were computed using all measurements for both rebar directions, for the entrance ramp, second level, third level, and helix were determined to be 3.2, 3.0, 3.5, and 4.1 in., respectively.

Table 4-1: Schmidt Rebound Numbers for Ground Level

X Coordinate (ft)	Y Coordinate (ft)	Schmidt Rebound Numbers									
0	0	54	56	56	52	54	52	54	60	60	54
0	10	56	56	60	54	60	54	58	54	58	54
0	20	54	54	54	52	54	56	52	56	54	54
0	30	54	56	54	50	54	56	54	54	52	54
20	0	54	54	56	56	52	50	52	54	52	52
20	10	56	52	50	54	56	56	56	52	52	52
20	20	64	56	56	58	58	64	58	54	54	58
20	30	54	56	54	58	56	56	56	54	54	58
40	0	56	52	56	56	48	52	54	54	56	56
40	10	62	56	56	52	60	58	58	58	56	58
40	20	56	56	58	52	54	56	58	58	54	50
40	30	56	56	54	48	52	52	52	54	58	54

Table 4-2: Schmidt Rebound Numbers for Entrance Ramp

X Coordinate (ft)	Y Coordinate (ft)	Schmidt Rebound Numbers									
5.5	5.5	62	60	60	69	63	58	66	68	58	66
5.5	15.5	64	62	59	61	60	60	60	60	60	62
5.5	25.5	59	69	58	64	58	57	57	60	60	64
16.75	5.5	57	59	58	57	63	59	60	57	59	58
16.75	15.5	68	64	59	68	61	60	62	66	63	60
16.75	25.5	58	61	61	61	60	60	61	62	64	62
28	5.5	62	60	58	62	59	62	61	60	63	57
28	15.5	61	63	61	61	64	62	62	65	60	62
28	25.5	61	64	60	62	60	61	63	58	61	64
45.5	5.5	57	68	57	52	60	57	59	54	52	55
45.5	15.5	52	50	52	52	53	50	52	53	62	54
45.5	25.5	54	58	52	54	52	54	55	57	55	56
57.75	5.5	54	54	60	53	57	52	54	51	54	55
57.75	15.5	57	55	59	57	60	57	54	54	55	58
57.5	25.5	61	57	55	58	54	62	63	64	54	56
70	5.5	57	56	65	62	69	58	60	56	58	58
70	15.5	62	57	60	60	68	65	68	64	58	61
70	25.5	62	59	61	65	58	58	57	68	63	61

Table 4-3: Schmidt Rebound Numbers for Second Level

X Coordinate (ft)	Y Coordinate (ft)	Schmidt Rebound Numbers									
5	5	58	56	54	54	54	58	54	54	56	56
5	15	64	58	54	58	58	54	56	60	64	66
5	25	62	66	60	58	56	48	56	54	62	58
5	35	54	52	54	44	56	54	60	52	56	56
15	5	60	56	70	62	62	58	64	60	60	-
15	15	52	54	62	48	60	58	54	56	56	56
15	25	52	58	62	54	56	56	48	58	54	58
15	35	52	52	54	52	56	44	50	46	52	50
25	5	62	64	58	58	56	58	58	60	60	56
25	15	60	48	58	58	60	52	48	58	62	60
25	25	54	64	62	58	58	54	60	54	60	58
25	35	48	50	42	58	52	52	54	46	54	64
35	5	56	56	64	52	52	54	58	60	58	58
35	15	58	60	60	60	62	56	58	58	68	62
35	25	58	56	56	58	58	60	68	68	60	56
35	35	48	48	58	52	56	56	54	44	58	56
45	5	56	58	58	52	58	54	54	58	66	68
45	15	58	68	54	54	58	48	58	62	58	56
45	25	52	54	58	60	68	50	54	58	58	56
45	35	50	48	60	60	54	56	50	56	54	54

Table 4-4: Schmidt Rebound Numbers for Third Level

X Coordinate (ft)	Y Coordinate (ft)	Schmidt Rebound Numbers									
0	0	52	54	54	56	58	48	50	66	50	56
0	10	54	52	52	50	52	52	54	52	62	60
0	20	52	54	50	52	52	56	56	52	48	54
0	30	58	58	56	52	52	54	56	52	54	58
10	0	54	52	56	54	58	58	54	52	54	54
10	10	56	54	54	54	54	56	56	54	56	56
10	20	56	56	58	56	58	60	56	58	58	60
10	30	54	60	52	68	54	54	52	54	50	54
20	0	54	60	52	52	54	54	54	50	60	54
20	10	54	52	54	62	58	54	66	52	56	54
20	20	52	58	56	60	56	56	56	60	56	54
20	30	60	58	58	54	54	58	56	62	56	54
30	0	58	54	56	58	54	56	54	60	58	56
30	10	54	58	54	56	54	52	54	56	62	56
30	20	54	54	52	50	56	58	52	62	52	50
30	30	58	58	58	54	56	54	54	56	58	54
40	0	50	50	54	52	52	54	54	54	52	52
40	10	56	58	52	54	52	54	56	56	56	56
40	20	60	54	54	58	60	54	56	58	54	54
40	30	60	54	56	58	58	58	56	58	64	58

Table 4-5 Schmidt Rebound Numbers for Helix

Level of Parking Structure	X Coordinate (ft)	Y Coordinate (ft)	Schmidt Rebound Numbers									
1	84	22	55	56	52	54	52	56	55	61	64	56
2	12	36	60	56	58	54	64	60	60	57	57	67
3	9	41	53	49	59	59	53	57	44	57	57	58

Table 4-6: Average Schmidt Rebound Numbers

Testing Area	Average Schmidt Rebound Number	Estimated Compressive Strength (psi)
Ground Level	55	7933
Entrance Ramp	59	9159
Second Level	57	8378
Third Level	55	8017
Helix	57	8400

Table 4-7: Cover Depth Measurements for Entrance Ramp

Coordinate (ft)		Cover Depth (in.) for Indicated Rebar Direction	
X	**Y**	**North-South**	**East-West**
5.5	5.5	4.1	4.7
5.5	15.5	3.7	4.6
5.5	25.5	3.9	5.0
16.75	5.5	2.8	3.2
16.75	15.5	2.4	2.6
16.75	25.5	2.6	2.5
28.0	5.5	2.8	2.6
28.0	15.5	2.7	2.6
28.0	25.5	2.3	2.4
45.5	5.5	2.5	2.3
45.5	15.5	2.2	2.6
45.5	25.5	2.6	2.6
57.75	5.5	2.9	2.9
57.75	15.5	2.8	2.6
57.5	25.5	2.4	2.9
70.0	5.5	3.7	4.2
70.0	15.5	4.2	4.8
70.0	25.5	4.1	4.6
Average		3.0	3.3
Overall Average		3.2	

Table 4-8: Cover Depth Measurements for Second Level

Coordinate (ft)		Cover Depth (in.) for Indicated Rebar Direction	
X	**Y**	**North-South**	**East-West**
5.0	5.0	2.6	2.3
5.0	15.0	2.4	2.3
5.0	25.0	2.4	1.8
5.0	35.0	2.9	2.8
15.0	5.0	2.5	2.2
15.0	15.0	5.3	5.2
15.0	25.0	4.5	2.4
15.0	35.0	2.6	2.8
25.0	5.0	2.9	2.8
25.0	15.0	5.4	5.1
25.0	25.0	4.5	3.0
25.0	35.0	2.9	2.5
35.0	5.0	3.4	2.6
35.0	15.0	3.0	3.9
35.0	25.0	2.1	2.5
35.0	35.0	1.8	2.1
45.0	5.0	2.8	2.8
45.0	15.0	2.9	3.1
45.0	25.0	3.1	3.0
45.0	35.0	2.2	2.1
Average		3.1	2.8
Overall Average		3.0	

Table 4-9: Cover Depth Measurements for Third Level

Coordinate (ft)		Cover Depth (in.) for Indicated Rebar Direction	
X	Y	North-South	East-West
0.0	0.0	2.8	3.3
0.0	10.0	4.3	4.7
0.0	20.0	3.9	5.1
0.0	30.0	3.1	2.3
20.0	0.0	3.0	3.1
20.0	10.0	5.8	4.5
20.0	20.0	5.8	4.8
20.0	30.0	3.3	2.8
40.0	0.0	2.1	2.0
40.0	10.0	3.2	3.1
40.0	20.0	3.1	3.5
40.0	30.0	2.1	1.9
Average		3.5	3.4
Overall Average		3.5	

Table 4-10: Cover Depth Measurements for Helix

Level of Parking Structure	Coordinate (ft)		Cover Depth (in.) for Indicated Rebar Direction	
	X	Y	North-South	East-West
1	84.0	22.0	4.5	4.0
2	12.0	36.0	4.7	4.0
3	9.0	41.0	3.9	3.3
Average			4.4	3.8
Overall Average			4.1	

4.3 Laboratory Testing Results

The results of chloride concentration, modulus of elasticity, electrical impedance, rapid chloride permeability, splitting tensile strength, compressive strength, and carbonation depth testing are presented in the following sections. Pictures of the cores taken before any testing occurred are provided in the appendix.

4.3.1 Chloride Concentration Testing

Chloride concentration data are presented in Table 4-11 through Table 4-16, in which a hyphen indicates an absence of data or designates an entry as not applicable. As evidence of the high chloride ion exposure experienced by the parking structure, the chloride concentrations near the surface were generally high. However, attributable to the low permeability of the concrete,

Table 4-11: Chloride Concentration Data for Ground Level

Coordinate (ft)		Chloride Concentration (lb Cl^-/yd^3) for Indicated Depth Interval (in.)							Cover (in.)	Description
X	Y	0-1	1-2	2-3	3-4	4-5	5-6	6-7		
10	5	17.3	1.5	1.0	1.5	1.8	2.3	-	No Rebar	High Spot
18	25	7.4	5.1	3.0	2.5	2.9	3.3	-	No Rebar	Wheel Path (Not Cracked)
18	25	24.0	4.4	1.3	0.9	0.9	1.7	-	No Rebar	Wheel Path (Not Cracked)
22	23	9.6	4.6	1.2	1.3	1.6	2.2	-	No Rebar	Between Wheel Paths
38	21	1.2	0.2	0.4	1.1	1.9	-	-	No Rebar	Parking Stall
40	5	5.8	0.7	1.0	2.1	3.6	5.1	-	No Rebar	Low Spot
Average		10.9	2.8	1.3	1.5	2.1	2.9	-	-	-

Table 4-12: Chloride Concentration Data for Entrance Ramp

Coordinate (ft)		Chloride Concentration (lb Cl^-/yd^3) for Indicated Depth Interval (in.)							Cover (in.)	Description
X	Y	0-1	1-2	2-3	3-4	4-5	5-6	6-7		
8	18	43.1	11.8	8.1	7.9	7.5	6.6	9.1	3.7	Cracked
8	18	19.9	0.7	0.4	0.3	0.3	0.3	-	3.7	Not Cracked
22	4	25.1	14.7	11.3	9.5	8.1	10.1	8.6	2.4	Cracked
22	4	18.4	0.8	0.9	0.4	0.4	1.2	0.9	2.4	Not Cracked
24	20	19.1	9.2	7.8	6.4	6.1	7.9	14.6	2.3	Cracked
24	20	8.7	0.3	0.3	0.2	0.2	0.3	0.3	2.3	Not Cracked
41	9	18.0	4.6	4.9	4.6	3.8	2.1	3.7	2.2	Cracked
41	9	14.3	0.5	0.2	0.3	0.3	0.4	-	2.2	Not Cracked
54	15	16.9	4.4	2.8	3.3	4.1	3.1	4.3	2.4	Cracked
54	15	15.2	0.6	0.4	0.4	0.3	0.3	0.2	2.4	Not Cracked
72	20	11.9	7.2	4.5	4.5	4.4	4.2	2.8	3.7	Cracked
72	20	15.0	1.5	0.2	0.2	0.2	0.2	0.3	3.7	Not Cracked
Average		22.3	8.6	6.6	6.0	5.7	5.7	7.2	2.8	Cracked
		15.2	0.7	0.4	0.3	0.3	0.4	0.4	2.8	Not Cracked

Table 4-13: Chloride Concentration Data for Second Level

Coordinate (ft)		Chloride Concentration (lb Cl^-/yd^3) for Indicated Depth Interval (in.)							Cover (in.)	Description
X	Y	0-1	1-2	2-3	3-4	4-5	5-6	6-7		
5	7	15.9	10.9	10.2	9.9	5.9	2.3	-	2.3	Cracked
5	7	11.5	0.5	0.3	0.3	0.3	0.4	-	2.3	Not Cracked
18	25	8.0	0.3	0.3	0.2	0.3	0.5	-	2.4	Cracked
18	25	22.8	0.6	0.3	0.3	0.3	0.3	-	2.4	Not Cracked
33	26	16.0	7.4	8.6	9.8	8.8	5.7	-	2.1	Cracked
33	26	12.3	0.3	0.3	0.2	0.2	0.2	-	2.1	Not Cracked
Average		13.3	6.2	6.4	6.6	5.0	2.8	-	2.2	Cracked
		15.5	0.4	0.3	0.3	0.2	0.3	-	2.2	Not Cracked

Table 4-14: Chloride Concentration Data for Third Level

Coordinate (ft)		Chloride Concentration (lb Cl^-/yd^3) for Indicated Depth Interval (in.)							Cover (in.)	Description
X	Y	0-1	1-2	2-3	3-4	4-5	5-6	6-7		
10	10	43.9	1.4	0.3	0.2	0.4	0.1	-	4.3	Not Cracked
10	20	16.2	0.5	0.4	0.3	0.3	0.2	-	3.9	Not Cracked
20	10	38.5	0.5	0.3	0.3	0.3	0.3	-	4.5	Not Cracked
20	20	15.8	1.4	0.3	0.4	0.3	0.3	-	4.8	Not Cracked
30	10	15.6	1.1	0.2	0.3	0.0	0.2	-	3.1	Not Cracked
30	20	9.4	0.5	0.2	0.4	0.3	0.3	-	3.1	Not Cracked
Average		23.2	0.9	0.3	0.3	0.3	0.2	-	3.9	Not Cracked

Table 4-15: Chloride Concentration Data for Helix

Level	Coordinate (ft)		Chloride Concentration (lb Cl^-/yd^3) for Indicated Depth Interval (in.)							Cover (in.)	Description
	X	Y	0-1	1-2	2-3	3-4	4-5	5-6	6-7		
1	84	22	43.2	11.7	12.6	13.5	-	-	-	4.0	Cracked
	84	22	14.1	0.5	0.3	0.3	0.4	-	-	4.0	Not Cracked
2	12	36	21.1	14.0	7.5	7.2	12.7	-	-	4.0	Cracked
	12	36	22.0	1.0	0.3	0.6	0.3	9.4	-	4.0	Not Cracked
3	9	41	18.0	11.1	8.3	8.0	-	-	-	3.3	Cracked
	5	41	23.7	1.5	0.3	0.4	2.7	-	-	3.3	Not Cracked
Average			27.4	12.3	9.5	9.6	12.7	-	-	3.8	Cracked
			19.9	1.0	0.3	0.4	1.2	9.4	-	3.8	Not Cracked

Table 4-16: Comparison of Average Chloride Concentrations for Uncracked and Cracked Concrete

Description	Chloride Concentration (lb Cl^-/yd^3) for Indicated Depth Interval (in.)						
	0-1	**1-2**	**2-3**	**3-4**	**4-5**	**5-6**	**6-7**
Uncracked Concrete	16.96	1.16	0.51	0.57	0.81	2.65	0.43
Cracked Concrete	21.03	9.05	7.46	7.41	7.78	4.25	7.16
Percent Increase in Chloride Concentration (%)	124	777	1468	1296	965	161	1666

the chloride concentrations at the depth of the rebar, where applicable, were less than the corrosion initiation threshold value of 2.0 lb Cl^-/yd^3 of concrete for exposed steel at all test locations where the concrete was not cracked. For locations that were cracked, the deeper penetration of chloride ions was very apparent. Table 4-16 specifically compares the chloride concentrations of cracked and uncracked concrete and shows that, across all depth intervals, the chloride concentration of cracked concrete was 124% to 1666% greater, on average, than the chloride concentration of uncracked concrete. Specifically, for the depth interval of 3 in. to 4 in., which is consistent with the measured cover depths, the average chloride concentration of the cracked locations was 7.4 lb Cl^-/yd^3, while the average chloride concentration of the uncracked locations was 0.6 lb Cl^-/yd^3. These results clearly highlight the negative effects of cracking on chloride ion penetration in concrete. Also for the depth interval of 3 in. to 4 in., the average chloride concentrations of the concrete comprising silica fume and the concrete without silica fume in uncracked testing locations were 0.3 lb Cl^-/yd^3 and 1.5 lb Cl^-/yd^3, respectively.

4.3.2 Modulus of Elasticity Testing

Modulus of elasticity values are presented in Table 4-17 for all concrete cores. The average modulus ranged from 3061 ksi to 5761 ksi for the test areas, and the average modulus values for concrete comprising silica fume and concrete without silica fume were 4415 ksi and 4577 ksi, respectively.

4.3.3 Electrical Impedance Testing

Electrical impedance values are shown in Table 4-18 for all of the concrete cores. The average normalized impedance ranged from 18,724 ohm/in. to 271,343 ohm/in. for the test areas, and the average normalized impedance values for concrete comprising silica fume and concrete without silica fume were 94,589 ohm/in. and 20,923 ohm/in., respectively. Cores “Helix L1” and “Helix L3” had significantly higher electrical impedance values than the other cores.

4.3.4 Rapid Chloride Permeability Testing

RCPT values are shown in Table 4-19 for at least one concrete core sampled from each level and the helix. The average charge passed in the RCPT ranged from 162 coulombs to 1448 coulombs for the test areas, and the average values of charge passed for concrete comprising silica fume and concrete without silica fume were 787 coulombs and 1343 coulombs, respectively. According to Table 4-20, which shows chloride permeability ratings with relation to the charge passed (Joshi and Chan 2002), these averages correlate to permeability ratings of “Very Low” and “Low,” respectively.

4.3.5 Splitting Tensile Strength Testing

Splitting tensile strength data are provided in Table 4-21 for at least one concrete core sampled from each level and the helix. After reaching their peak loads, specimens broke suddenly in brittle failure, with the load immediately decreasing to zero. The average splitting tensile strength ranged from 732 psi to 1031 psi for the test areas, and the average splitting tensile strengths for concrete comprising silica fume and concrete without silica fume were 867 psi and 921 psi, respectively. Figure 4-1 shows a typical core after splitting tensile strength testing.

Table 4-17: Modulus of Elasticity Data

Core Identification Number	Weight (lb)	Length (in.)	Unit Weight (lb/ft^3)	Frequency (Hz)	Modulus of Elasticity (ksi)
G 10-5	5.0	6.1	134.0	12190	4459
G 18-24	4.4	5.2	137.4	14591	4823
G 40-5	4.8	5.7	137.6	12929	4450
Lane 1	3.4	4.0	136.7	18091	4238
Lane 2	4.8	4.9	153.1	14865	4888
Lane 3	4.2	4.8	138.5	12675	3061
Lane 4	4.1	4.7	139.3	13021	3132
Lane 5	4.3	5.0	134.1	15145	4585
Lane 6 (Top)	2.2	2.7	137.7	27067	4368
Lane 6 (Bottom)	1.8	2.1	136.2	33372	3965
L2 5-5	6.7	7.9	137.9	8651	3893
L2 17-25	6.5	7.8	135.1	9884	4853
L2 32-25	4.9	5.8	136.7	13206	4878
L3 10-10	5.0	5.9	138.1	13359	5151
L3 21-20	6.4	8.4	133.3	9395	4975
L3 30.5-9.5	8.3	9.6	136.8	7928	4756
Helix L1	2.7	3.4	133.0	24889	5761
Helix L2	3.7	4.2	139.1	15325	3425
Helix L3	2.4	2.9	132.4	26387	4717

Table 4-18: Electrical Impedance Data

Core Identification Number	Electrical Impedance (Ohm)	Length (in.)	Normalized Electrical Impedance (Ohm/in.)
G 10-5	123000	6.1	20119
G 18-24	125500	5.2	23924
G 40-5	106400	5.7	18724
Lane 1	258000	4.0	64881
Lane 2	594000	4.9	120928
Lane 3	518000	4.8	108108
Lane 4	320000	4.7	68013
Lane 5	419000	5.0	84006
Lane 6 (Top)	325000	2.7	120874
Lane 6 (Bottom)	108000	2.1	51706
L2 5-5	293000	7.9	36922
L2 17-25	543000	7.8	69300
L2 32-25	252000	5.8	43116
L3 10-10	160000	5.9	27091
L3 21-20	448500	8.4	53382
L3 30.5-9.5	312200	9.6	32484
Helix L1	861000	3.4	252031
Helix L2	457000	4.2	109232
Helix L3	793000	2.9	271343

Table 4-19: Rapid Chloride Permeability Data

Core Identification Number	Charge Passed (coulombs)	Permeability Class
G 40-5	1343	Low
Lane 3	404	Very Low
Lane 4	162	Very Low
L2 17-25	1151	Low
L3 17-20	772	Very Low
Helix 1	1448	Low

Table 4-20: Ratings of Chloride Permeability

Charge Passed (coulombs)	Chloride Permeability
> 4000	High
2000 to 4000	Moderate
1000 to 2000	Low
100 to 1000	Very Low
< 100	Negligible

Table 4-21: Splitting Tensile Strength Data

Core Identification Number	Length (in.)	Diameter (in.)	Peak Load (lb)	Splitting Tensile Strength (psi)
G 18-24	2.36	3.68	12565	921
Lane 1	2.36	3.72	12805	927
Lane 6 (Top)	2.36	3.64	12365	916
Lane 6 (Bottom)	2.36	3.72	10365	752
L2 32-25	2.36	3.67	11485	844
L3 10-10	2.36	3.68	14070	1031
Helix L3	2.92	3.73	12530	732

Figure 4-1: Typical core after splitting tensile strength testing.

4.3.6 Compressive Strength Testing

Compressive strength data are shown in Table 4-22 for at least one concrete core sampled from each level and the helix. As in splitting tensile strength testing, all specimens exhibited a brittle failure. The average compressive strength ranged from 6489 psi to 10611 psi for the test areas, and the average compressive strengths for concrete comprising silica fume and concrete without silica fume were 9049 psi and 6489 psi, respectively. Figure 4-2 shows a typical core after compressive strength testing.

4.3.7 Carbonation Depth Measurements

Carbonation depth measurements are shown in Table 4-23 for at least two concrete cores sampled from each level and the helix. The average carbonation depth ranged from 0.00 in. to 0.39 in. for the test areas, and the average carbonation depths for concrete comprising silica fume and concrete without silica fume were 0.07 in. and 0.13 in., respectively. These data indicate that the concrete had very low susceptibility to carbonation-induced corrosion of the embedded reinforcing steel even after 30 years of service.

4.4 Summary

The results of field testing included data obtained from visual inspection, chain dragging, Schmidt hammer testing, and cover depth measurements, while the results of laboratory testing included data obtained from chloride concentration, modulus of elasticity, electrical impedance, rapid chloride permeability, splitting tensile strength, compressive strength, and carbonation depth testing.

Regarding field testing, as documented in a previous report, the average crack density within the parking structure ranged from 0.002 to 0.095 ft/ft^2, and no potholes were observed in any of the decks. During visual inspection, no differences were apparent between concrete comprising silica fume and concrete without silica fume. The average estimated compressive strengths of concrete comprising silica fume and concrete without silica fume were 8488 psi and 7933 psi, respectively. The average depths to the top of the rebar, which were computed using all measurements for both rebar directions, for the entrance ramp, second level, third level, and helix were determined to be 3.2, 3.0, 3.5, and 4.1 in., respectively.

Regarding laboratory testing, for the depth interval of 3 in. to 4 in., which is consistent with the measured cover depths, the average chloride concentration of the cracked locations was 7.4 lb Cl^-/yd^3, while the average chloride concentration of the uncracked locations was 0.6 lb Cl^-/yd^3. Also for the depth interval of 3 in. to 4 in., the average chloride concentrations of the concrete comprising silica fume and the concrete without silica fume in uncracked testing locations were 0.3 lb Cl^-/yd^3 and 1.5 lb Cl^-/yd^3, respectively. The average modulus ranged from 3061 ksi to 5761 ksi for the test areas, and the average modulus values for concrete comprising silica fume and concrete without silica fume were 4415 ksi and 4577 ksi, respectively. The average normalized impedance ranged from 18,724 ohm/in. to 271,343 ohm/in. for the test areas, and the average normalized impedance values for concrete comprising silica fume and concrete without silica fume were 94,589 ohm/in. and 20,923 ohm/in., respectively. The average charge passed in the RCPT ranged from 162 coulombs to 1448 coulombs for the test areas, and the average values of charge passed for concrete comprising silica fume and concrete without silica fume were 787 coulombs and 1343 coulombs, respectively; these averages correlate to permeability ratings of "Very Low" and "Low," respectively. The average splitting tensile strength ranged from 732 psi

Table 4-22: Compressive Strength Data

Core Identification Number	Diameter (in.)	Peak Load (lb)	Compressive Strength (psi)
G 10-5	3.67	68630	6489
Lane 2	3.73	115920	10611
Lane 5	3.74	81835	7439
L2 5-5	3.68	96630	9095
L3 30.5-9.5	3.73	92670	8494
Helix L2	3.74	105445	9606

Table 4-23: Carbonation Depth Measurements

Core Identification Number	Carbonation Depth (in.)
G 10-5	0.00
G 18-24	0.39
Lane 1	0.00
Lane 2	0.13
Lane 5	0.09
Lane 6 (Top)	0.31
Lane 6 (Bottom)	0.00
L2 5-5	0.00
L2 32-25	0.00
L3 10-10	0.00
L3 30.5-9.5	0.13
Helix L2	0.00
Helix L3	0.17

Figure 4-2: Typical core after compressive strength testing.

to 1031 psi for the test areas, and the average splitting tensile strengths for concrete comprising silica fume and concrete without silica fume were 867 psi and 921 psi, respectively. The average compressive strength ranged from 6489 psi to 10611 psi for the test areas, and the average compressive strengths for concrete comprising silica fume and concrete without silica fume were 9049 psi and 6489 psi, respectively. The average carbonation depth ranged from 0.00 in. to 0.39 in. for the test areas, and the average carbonation depths for concrete comprising silica fume and concrete without silica fume were 0.07 in. and 0.13 in., respectively; these data indicate that the concrete had very low susceptibility to carbonation-induced corrosion of the embedded reinforcing steel even after 30 years of service.

In summary, the concrete comprising silica fume exhibited higher values than concrete without silica fume in Schmidt hammer, electrical impedance, and compressive strength testing and lower values than concrete without silica fume in chloride concentration, rapid chloride permeability, and carbonation depth testing; these results suggest that concrete comprising silica fume would provide greater strength and durability than concrete without silica fume. As exceptions, concrete without silica fume exhibited marginally higher values than concrete comprising silica fume in modulus of elasticity and splitting tensile strength testing; while a lower modulus of elasticity for concrete comprising silica fume may be less desirable from a strength perspective, it may actually be more desirable from a durability perspective to the degree that concrete having a lower modulus of elasticity would be expected to be less brittle and therefore less likely to crack. Overall, the results of this research indicate that the use of silica fume in the concrete mixture provided improved performance of the parking structure.

5 CONCLUSION

5.1 Summary

The objective of this research was to quantify the benefits of silica fume through a detailed investigation of the concrete decks within the now-demolished Salt Lake City International Airport parking structure, which was constructed in 1991, after it had been in service for almost 30 years. Areas on the ground level, the entrance ramp to the first level, the second level, the third level, and the east helix were selected for testing. Several field tests were performed to evaluate each of the five areas within the parking structure. These tests included visual inspection, chain dragging, Schmidt hammer testing, cover depth measurements, chloride concentration sampling, and coring. Concrete samples were removed from a total of 19 coring locations and 36 chloride concentration sampling locations within the parking structure for additional testing in the BYU Highway Materials Laboratory. The various non-destructive and destructive tests performed in the laboratory included chloride concentration, impact resonance, electrical impedance, rapid chloride permeability, splitting tensile strength, compressive strength, and carbonation depth tests.

5.2 Findings

The results of field testing included data obtained from visual inspection, chain dragging, Schmidt hammer testing, and cover meter readings, while the results of laboratory testing included data obtained from chloride concentration, modulus of elasticity, electrical impedance, rapid chloride permeability, splitting tensile strength, compressive strength, and carbonation depth testing.

Regarding field testing, as documented in a previous report, the average crack density within the parking structure ranged from 0.002 to 0.095 ft/ft^2, and no potholes were observed in any of the decks. During visual inspection, no differences were apparent between concrete comprising silica fume and concrete without silica fume. The average estimated compressive strengths of concrete comprising silica fume and concrete without silica fume were 8488 psi and 7933 psi, respectively. The average depths to the top of the rebar for the entrance ramp, second level, third level, and helix was determined to be 3.2, 3.0, 3.5, and 4.1 in., respectively.

Regarding laboratory testing, for the depth interval of 3 in. to 4 in., which is consistent with the measured cover depths, the average chloride concentration of the cracked locations was 7.4 lb Cl^-/yd^3, while the average chloride concentration of the uncracked locations was 0.6 lb Cl^-/yd^3. Also for the depth interval of 3 in. to 4 in., the average chloride concentrations of the concrete comprising silica fume and the concrete without silica fume in uncracked testing locations were 0.3 lb Cl^-/yd^3 and 1.5 lb Cl^-/yd^3, respectively. The average modulus ranged from 3061 ksi to 5761 ksi for the test areas, and the average modulus values for concrete comprising silica fume and concrete without silica fume were 4415 ksi and 4577 ksi, respectively. The average normalized impedance ranged from 18,724 ohm/in. to 271,343 ohm/in. for the test areas, and the average normalized impedance values for concrete comprising silica fume and concrete without

silica fume were 94,589 ohm/in. and 20,923 ohm/in., respectively. The average charge passed in the RCPT ranged from 162 coulombs to 1448 coulombs for the test areas, and the average values of charge passed for concrete comprising silica fume and concrete without silica fume were 787 coulombs and 1343 coulombs, respectively; these averages correlate to permeability ratings of "Very Low" and "Low," respectively. The average splitting tensile strength ranged from 732 psi to 1031 psi for the test areas, and the average splitting tensile strengths for concrete comprising silica fume and concrete without silica fume were 867 psi and 921 psi, respectively. The average compressive strength ranged from 6489 psi to 10611 psi for the test areas, and the average compressive strengths for concrete comprising silica fume and concrete without silica fume were 9049 psi and 6489 psi, respectively. The average carbonation depth ranged from 0.00 in. to 0.39 in. for the test areas, and the average carbonation depths for concrete comprising silica fume and concrete without silica fume were 0.07 in. and 0.13 in., respectively; these data indicate that the concrete had very low susceptibility to carbonation-induced corrosion of the embedded reinforcing steel even after 30 years of service.

In summary, the concrete comprising silica fume exhibited higher average values than concrete without silica fume in Schmidt hammer, electrical impedance, and compressive strength testing and lower average values than concrete without silica fume in chloride concentration, RCPT, and carbonation depth testing; these results suggest that concrete comprising silica fume would provide greater strength and durability than concrete without silica fume. As exceptions, concrete without silica fume exhibited marginally higher values than concrete comprising silica fume in modulus of elasticity and splitting tensile strength testing; while a lower modulus of elasticity for concrete comprising silica fume may be less desirable from a strength perspective, it may actually be more desirable from a durability perspective to the degree that concrete having a lower modulus of elasticity would be expected to be less brittle and therefore less likely to crack. Overall, the results of this research indicate that the use of silica fume in the concrete mixture provided improved performance of the parking structure.

5.3 Recommendations

The results of this research suggest that concrete comprising silica fume should be expected to provide greater strength and durability than concrete without silica fume, assuming that the concrete mixture is designed, produced, placed, and cured properly. Where budgets permit, silica fume is therefore recommended for concrete projects for which high strength and durability are needed. Further research would be beneficial in comparing the performance of concrete comprising silica fume and concrete without silica fume in other applications, as well.

REFERENCES

Aliabdo, E., Elmoaty, A. 2012. *Reliability of Using Nondestructive Tests to Estimate Compressive Strength of Building Stones and Bricks.* Alexandria Engineering Journal, Vol 51, 193-203.

Bordelon, A., Clyde, M., Gwynn, T. 2021. *Salt Lake City Airport Parking Garage Visual Inspection Report*, Utah Department of Transportation – Research Division, UT-21.23.

Camarini, G., Bardella, P. 2013. *Chloride Penetration Depth in Silica Fume Concrete*, International Journal of Engineering and Technology, Vol. 5, No. 6.

Chia, K., Zhang, M. 2002. *Water Permeability and Chloride Penetrability of High-Strength Lightweight Aggregate Concrete*, Cement and Concrete Research, National University of Singapore. Vol 32, 639-645.

Cho, H., Ju, H., Oh, J., Lee, K., Hahm, K., Kim, K. 2016. *Estimation of Concrete Carbonation Depth Considering Multiple Influencing Factors on the Deterioration of Durability for Reinforced Concrete Structures*, Advances in Materials Science and Engineering, Vol 2016, Article 4814609.

Fidjestøl, H., Dåstøl, M. 2008. "The History of Silica Fume in Concrete – From Novelty to Key Ingredient in High Performance Concrete." Accessed March 23, 2022. http://www.ibracon.org.br/eventos/50cbc/plenarias/PER_FIDJESTOL.pdf.

Galishnikova, V., Abdo, S., Fawzy, A. 2020. *Influence of Silica Fume on the Pervious Concrete with Different Levels of Recycled Aggregates*, Magazine of Civil Engineering, 93(1), 71-82.

Gong, J., Zhu, L., Jiusu, L., Shi, D. 2020. *Silica Fume and Nanosilica Effects on Mechanical and Shrinkage Properties of Foam Concrete for Structural Application*, Advances in Materials Science and Engineering, https://doi.org/10.1155/2020/3963089.

Guthrie, W. S., and Yaede, J. M. 2013. "Internal Curing of Concrete Bridge Decks in Utah." Transportation Research Record: Journal of the Transportation Research Board, 2342(1), 121–128.

Hebdon, A. 2020. *Evaluation of Concrete Bridge Decks Comprising Twisted Steel Micro Rebar*, BYU Theses and Dissertations. 8788.

Henan Superior Abrasives Import and Export Co., Ltd. 2024. “95% Densified Silica Fume.” HSA Silica Fume. Accessed April 6, 2024. https://microsilica-fume.com/product/94-silica-fume

Hooton, R.D., Bentz, E., Kojundic, T. 2003. *Long-Term Chloride Penetration Resistance of Bridge Decks Made with Silica Fume Concretes*. Accessed September 3, 2022. http://www.life-365.org/images/deft-102010.pdf.

Jankovic, K., Ilic, A., Stojanovic, M. 2014. *The Influence of Silica Fume and Curing Regime on Some Properties of Concrete*, Romanian Journal of Materials, 44(1) 46-53.

Joshi, P., Chan, C. 2002. “Rapid Chloride Permeability Testing.” Accessed February 21, 2022. http://cdnassets.hw.net/c4/41/47e6d3f1444ebeabd060c3f1f887/rapid-chloride-permeability-testing-tcm45-590139.pdf.

Karakurt, C., Bayazit, Y. 2015. *Freeze-Thaw Resistance of Normal and High Strength Concretes Produced with Fly Ash and Silica Fume*, Advances in Materials Science and Engineering, http://dx.doi.org/10.1155/2015/830984.

King, D. 2012. *The Effect of Silica Fume on the Properties of Concrete as Defined in Concrete Society Report 74, Cementitious Materials*, Our World in Concrete and Structures, 37th Conference.

Klemetti, E. 2012. “What Happens to All That Volcanic Ash?” Accessed August 13, 2022. https://www.wired.com/2012/05/what-happens-to-all-that-volcanic-ash/.

Kulakowski, M., Pereira, F., Dal Molin, D. 2009. *Carbonation-Induced Reinforcement Corrosion in Silica Fume Concrete*, Construction and Building Materials, Vol 23, 1189-1195.

Leonhardt, F. 1988. “Cracks and Crack Control in Concrete Structures.” *PCI Journal*, Jul-Aug 1988, 124-145. https://www.pci.org/PCI_Docs/Design_Resources/Guides_and_manuals/references/bridge_design_manual/JL-88-July-August_Cracks_and_Crack_Control_in_Concrete_Structures.pdf.

Mindess, S. F., Young, J. F., and Darwin, D. F. 2003. “Fiber Reinforced Concrete.” Concrete, Second Edition, Prentice Hall, Upper Saddle River, NJ, 599-617.

Murthi, P., Sivakumar, V. 2008. *Studies on the Chloride Permeability of Fly Ash and Silica Fume Based Ternary Blended Concrete*, International Journal of Applied Engineering Research, Vol 3, 1481-1494.

Persson, B. 1998. *Seven-Year Study on the Effect of Silica Fume in Concrete*, Advn Cem Bas Mat, Vol 7, 139-155.

Roper, E. 2018. *Chloride Concentration and Blow-Through Analyses for Concrete Bridge Decks Rehabilitated Using Hydrodemolition*, BYU Theses and Dissertations. 7779.

Schmitt, T. R., and Darwin, D. 1995. "Cracking in Concrete Bridge Decks." University of Kansas, Center for Research, Lawrence, KS.

Silica Fume Association. 2005. "Silica Fume User's Manual." Accessed March 23. 2022. https://www.silicafume.org/pdf/silicafume-users-manual.pdf.

Wolsiefer, J. 1991. *Silica Fume Concrete: A Solution to Steel Reinforcement Corrosion in Concrete*, Symposium Paper. Vol 126, 527-558.

Yusuf, M. 2019. *Synergistic-Effect of Iron-Filing and Silica-Fume on the Absorption and Shrinkage of Cement Paste*, Magazine of Civil Engineering, 91(7), 16-26.

APPENDIX ORIGINAL CORES

Figure A-1: Core G 10-5

Figure A-2: Core G 18-24

Figure A-3: Core G 40-5

Figure A-4: Core Lane 1

Figure A-5: Core Lane 2

Figure A-6: Core Lane 3

Figure A-7: Core Lane 4

Figure A-8: Core Lane 5

Figure A-9: Core Figure 3 (Top)

Figure A-10: Core Lane 6 (Bottom)

Figure A-11: Core Lane 6 (Top and Bottom)

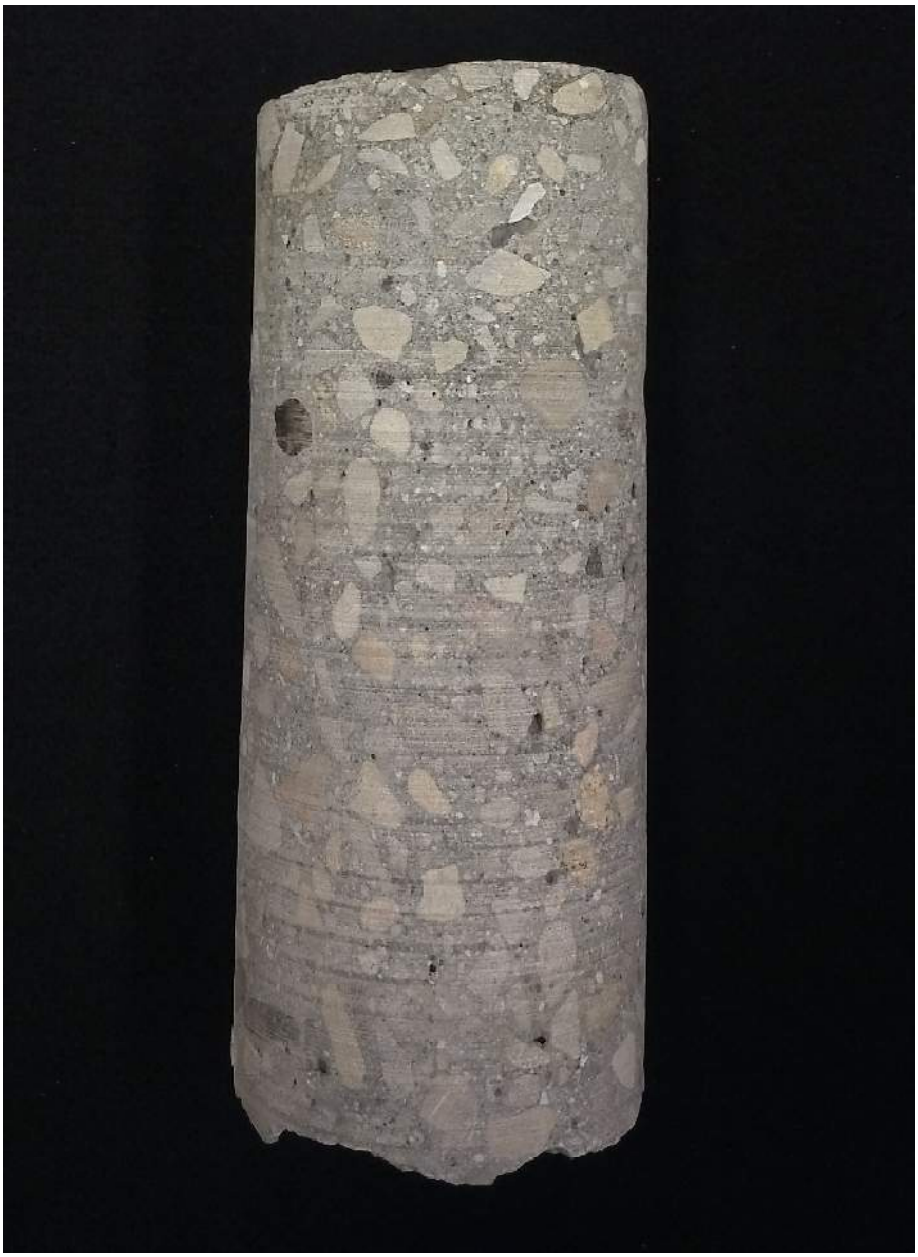

Figure A-12: Core L2 5-5

Figure A-13: Core L2 17-25

Figure A-14: Core L2 32-25

Figure A-15: Core L3 10-10

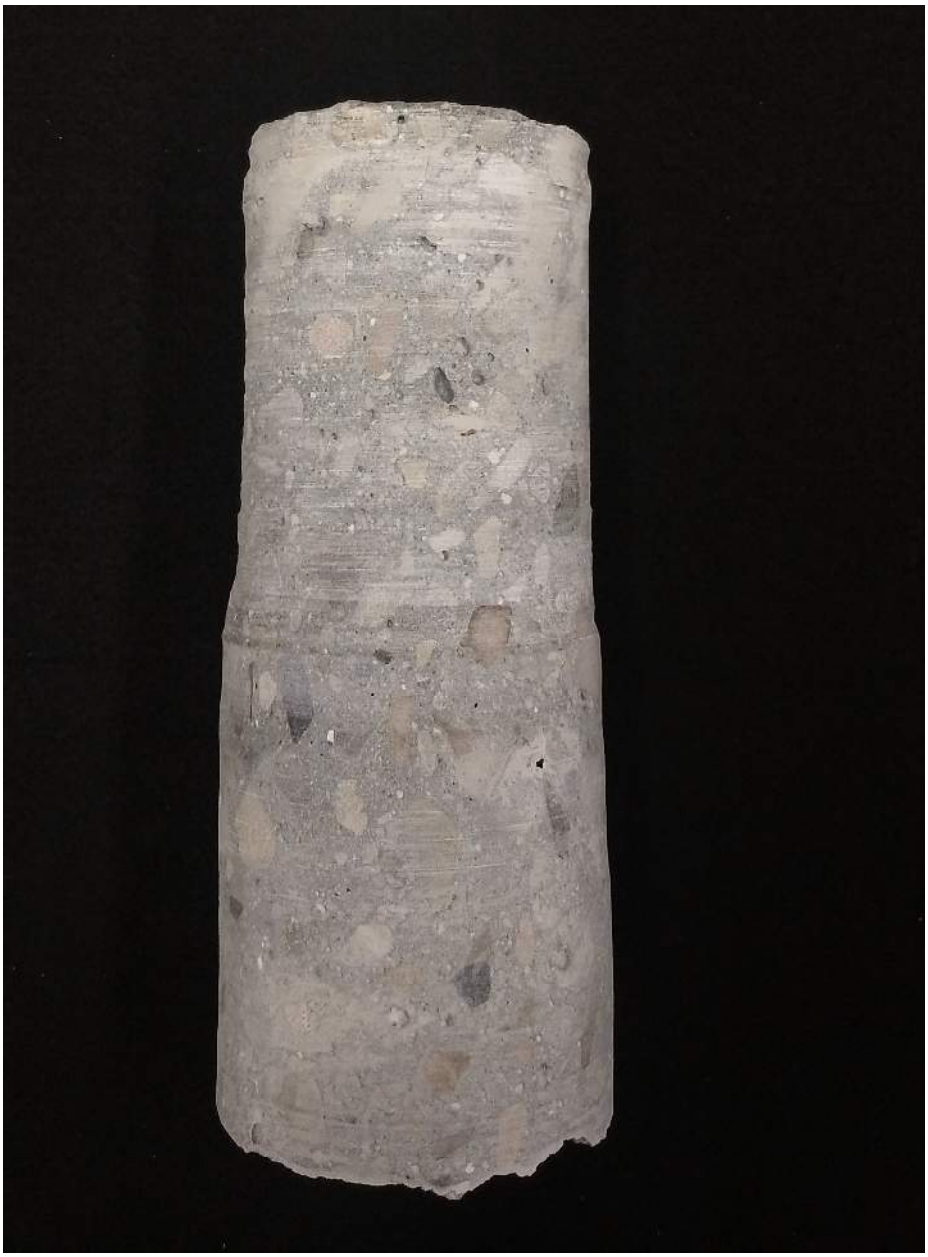

Figure A-16: Core L3 21-20

Figure A-17: Core L3 30.5-9.5

Figure A-18: Core Helix L1

Figure A-19: Core Helix L2

Figure A-20: Core Helix L3